MASTER COPY KEEP THIS COPY FOR REPRODUCTION PURPOSES

REPO

AD-A281 379

Form Approved
OMB No. 0704-0188

Public reporting burden for this col gathering and maintaining the data collection of information, including Davis Highway, Suite 1204, Arlingto

ding the time for reviewing instructions, searching existing data sources, end comments regarding this burden estimate or any other aspect of this ices, Directorate for information Operations and Reports, 1215 Jefferson work Reduction Project (0704-0188), Washington, DC 20503.

1. AGENCY USE ONLY (L

16 May 94

ORT TYPE AND DATES COVERED
Final 1 Mar 90-31 Jan 94

4. TITLE AND SUBTITLE

INFRARED/SUBMILLIMETER WAVE DOUBLE- RESONANCE STUDIES OF MOLECULAR COLLISION KINETICS

5. FUNDING NUMBERS

DAAL03-89-D-0002

6. AUTHOR(S)

David D. Skatrud

7. PERFORMING ORGANIZATION NAME(S) AND ADDRESS(ES)

Department of Physics
Duke University
Durham, NC 27705

8. PERFORMING ORGANIZATION REPORT NUMBER

9. SPONSORING / MONITORING AGENCY NAME(S) AND ADDRESS(ES)

U. S. Army Research Office
P. O. Box 12211
Research Triangle Park, NC 27709-2211

10. SPONSORING / MONITORING AGENCY REPORT NUMBER

ARO 27888.3-PH

11. SUPPLEMENTARY NOTES

The view, opinions and/or findings contained in this report are those of the author(s) and should not be construed as an official Department of the Army position, policy, or decision, unless so designated by other documentation.

12a. DISTRIBUTION / AVAILABILITY STATEMENT

Approved for public release; distribution unlimited.

12b. DISTRIBUTION CODE

13. ABSTRACT (*Maximum 200 words*)

Time-resolved, infrared/millimeter wave double resonance (IRMMWDR) techniques have been used to investigate roational and vibrational state changing collisions in molecules. Studies of several isotopic species of CH_3CL and CH_3F have led to a relatively simple model of the collisional energy transfer processes which accounts for an extemely large and diverse set of data. More specifically, about 350 IRMMWDR time-resolved data sets can be well predicted by a model with uses only five parameters for the rotational energy kinetics. Further, these five parameters are related to well known physical parameters.

94-21105

14. SUBJECT TERMS

submillimeter waves, far-infrared lasers, cw and transient multiresonance, molecular energy transfer

15. NUMBER OF PAGES

22

16. PRICE CODE

17. SECURITY CLASSIFICATION OF REPORT	18. SECURITY CLASSIFICATION OF THIS PAGE	19. SECURITY CLASSIFICATION OF ABSTRACT	20. LIMITATION OF ABSTRACT
UNCLASSIFIED	UNCLASSIFIED	UNCLASSIFIED	UL

NSN 7540-01-280-5500

Standard Form 298 (Rev. 2-89)
Prescribed by ANSI Std. 239-18
298-102

TITLE

Infrared/Submillimeter Wave Studies of Molecular Collision Kinetics

TYPE OF REPORT (TECHNICAL, FINAL, ETC.)

Final

AUTHOR (S)

David Skatrud

DATE

16 May 94

U. S. ARMY RESEARCH OFFICE

CONTRACT/GRANT NUMBER

DAAL03-89-D-002 / 27888PH

INSTITUTION

Department of Physics
Duke University

APPROVED FOR PUBLIC RELEASE;
DISTRIBUTION UNLIMITED.

STATEMENT OF PROBLEM STUDIED

Rotational and vibrational collisional energy transfer processes in polyatomic molecules have been investigated by means of infrared/millimeter wave double resonance (IRMMWDR) techniques. Previous studies have generally been limited to empirical descriptions of a limited subset of the most predominant channels because of the plethora of energetically available channels. An objective of the present study was to account for all significant relaxation pathways, and to describe them in terms of a few, hopefully physically meaningful, parameters. To this end, several isotopic species of CH_3F and CH_3Cl were studied in detail. More than 350 IRMMWDR time-resolved transitions were measured in CH_3Cl alone. These experimental observations constituted an extremely diverse set of data; they included more than 40 probe transitions with various angular momentum quantum states J and K, a number of different pump transitions and vibrational states, and a wide range of pressures. The parameters were determined by fitting the theoretical model on which they were based to the experimental data set by means of a nonlinear least squares fit. All of the rotational collisional transitions could be described using only five parameters, and these parameters are directly related to well known physical parameters.

Several features of the experimental apparatus were crucial to the success of the experiment. First, the millimeter-wave/submillimeter-wave probe is extremely sensitive to any deviations of rotational state population distributions from ambient, Boltzmann distributions. This extreme sensitivity allowed the measurements of small perturbations in the populations of states far from the pumped states. The sensitivity also provided a demanding test of the thermal nature of several of the theoretically proposed rotational energy transfer processes. Second, the essentially continuous tunability of the millimeter-wave/submillimeter-wave probe allowed selection of a wide range of rotational transitions. The resulting large data set provided much redundancy in verifying the theoretical model for the collisional energy transfer. Additional details on these and other features of the experimental set-up are described in more depth in appendix A.

SUMMARY OF THE MOST IMPORTANT RESULTS

The most rapid collisional process is that which changes the principal rotation quantum number J, while not changing any other quantum numbers. Owing to the large permanent electric dipole moment, the most rapid of these is the dipole collision process whose selection rules are $\Delta J = 0, \pm 1$. The cross-section for this process can be nearly an order-of-magnitude larger than the gas kinetic cross-section. Although significantly slower, higher order rates $\Delta J > 1$ were found to make significant contributions to rotational energy transfer because of their ability to affect large changes in quantum numbers in a single collision. All of the J-changing collisions were well modeled by both the statistical power gap fitting law and the infinite order sudden approximation with the assumption of a power law expression for the basis rates. Remarkably, by simply accounting for the difference in average thermal velocities between CH_3F and CH_3Cl, the same values for the pure ΔJ changing process could be used for both molecules.

Unlike with the ΔJ processes, significant differences were found between the ΔK processes of CH_3F and CH_3Cl (the projection of the angular momentum on the molecular axis is given by K). For symmetric top molecules with C_{3v} symmetry such as CH_3F and CH_3Cl, collisional rates which change K by other than multiples of three are extraordinarily slow since they require changes in the nuclear spin, which is very weakly coupled to molecular collisions. The earlier work on CH_3F demonstrated that rotational energy transfer involving ΔK processes were not selective in J or K aside from the above requirement that $\Delta K = 3n$. In addition it was found that these ΔK collisions were thermal in the sense that they distributed the transferred population according with a Boltzmann distribution at a single, ambient, thermal temperature. This was reflected in the experimental observation that all of the time-responses from the ΔK process had identical shapes. In contrast, it was found that the ΔK time-responses for CH_3Cl varied significantly; exhibiting differing degrees of a sharp feature which followed the termination of the pump pulse. This difference led to a generalization of the model for ΔK collisions. We found that all of the ΔK curves could be accurately modeled by simply allowing a time-varying temperature for the Boltzmann distribution. The time-varying temperature has the appealing features of being an exponential decay to ambient temperature from an initial temperature that is related to the difference between the energies of the pumped state and ambient. This straightforward and physically appealing model not only accounted for a wide variety of ΔK data in CH_3Cl, but it also satisfactorily reproduced the CH_3F ΔK data. The experimental and theoretical details of these results are discussed in depth in appendix A.

LIST OF PUBLICATIONS AND TECHNICAL REPORTS

David D. Skatrud, "Optically Pumped FIR Perturbation Laser," 15th International Conference on Infrared and Millimeter Waves, Conference Digest, SPIE Vol. 1514, Orlando, Florida, December 10-14, 1990.

Richard L. Crownover, Henry O. Everitt, Frank C. De Lucia, and David D. Skatrud, "Frequency Stability and Reproducibility of Optically Pumped Far-Infrared Lasers," Appl. Phys. Lett. **57**, 2882-2884 (1990).

Travis W. Pape, Frank C. De Lucia, and David D. Skatrud, "Time-resolved double resonance study of J- and K- changing rotational collisional processes in CH_3Cl," J. Chem. Phys. **100**, 5666-5683 (1994).

SCIENTIFIC PERSONNEL

David Skatrud
Travis Pape, Ph. D. - December 93

REPORT OF INVENTIONS

None.

APPENDIXES

A1 - "Time-resolved double resonance study of J- and K- changing rotational collisional processes in CH_3Cl," J. Chem. Phys. **100**, 5666-5683 (1994)

Time-resolved double resonance study of J- and K-changing rotational collisional processes in CH_3Cl

Travis W. Pape, Frank C. De Lucia,[a] and David D. Skatrud[b]
Department of Physics, Duke University, Box 90305, Durham, North Carolina 27708

(Received 20 August 1993; accepted 4 January 1994)

Time-resolved double resonance spectroscopy using infrared pump radiation and millimeter-wave and submillimeter-wave probe radiation (IRMMDR) has been used to study rotational energy transfer (RET) in CH_3Cl. A collisional energy transfer model using only five parameters for RET plus those needed for vibrational processes is shown to accurately model 350 IRMMDR time responses for two different pump states and 43 probe transitions covering a wide range of rotational states. Previous studies in this laboratory have revealed that J- and K-changing RET have vastly different characters in CH_3F [J. Chem. Phys. 92, 6480 (1990)]. Both J- and K-changing RET were accurately modeled with four parameters—one for dipole–dipole collisions, two for the ΔJ scaling law, and one for the cumulative rate of K-changing collisions. As was found for CH_3F, J-changing rotational collision rates in CH_3Cl are modeled accurately by both the statistical power gap (SPG) law and the infinite order sudden approximation using a power law expression for the basis rates (IOS-P). However, in contrast to CH_3F, where all IRMMDR time responses for K-changing collisions have the same shape, many time responses of CH_3Cl states populated by K-changing collisions contain an additional early time feature (ETF) that varies with pump and probe states. Nonetheless, a simple generalization of the previously reported model for K-changing collisions is shown to account for all of the additional features observed in CH_3Cl. Rather than observing a fixed temperature for K-changing collisions as was the case for CH_3F, the temperature is found to be a function of time for CH_3Cl. Moreover, the two new parameters this adds to the RET model are related to known physical quantities. A qualitative argument of K-changing collisions based on a classical picture is offered to explain the difference between the measured J- and K-changing state-to-state rates in CH_3Cl.

I. INTRODUCTION

Double resonance spectroscopy using infrared pump radiation and probe radiation in the millimeter-wave to submillimeter-wave range (IRMMDR) has been shown to be a powerful technique for the study of both rotational and vibrational state-changing collisions in small polyatomic molecules.[1-7] In our earlier time-resolved IRMMDR investigations of CH_3F, we found that J-changing collisions (for $v_3=1$ of CH_3F, $\Delta J=n$, $\Delta K=0$, where n is an integer) are modeled well by both the statistical power gap (SPG) fitting law and the infinite order sudden approximation assuming a power law expression for the basis rates (IOS-P).[6] While dipole–dipole rates were the most rapid, quantum number changes of up to $|\Delta J|=10$ were observed in the data. In contrast, K-changing rotational collisions (for $v_3=1$ of CH_3F, $\Delta J=m$, $\Delta K=3n$, where m and n are integers) were *not* found to be selective in either J or K beyond the symmetry preservation propensity rule discussed by Oka, $\Delta K=3n$ for symmetric top molecules of C_{3v} symmetry.[8] These K-changing collisions were found to be capable of causing large changes of a molecule's rotational energy in a single collision, populating rotational states in proportion to their contributions to the rotational partition function.[5] In other words, the rotational states of the same symmetry type and vibrational state as the pumped state maintain a Boltzmann population distribution at all times. We refer to a collisional process as thermal if it populates a group of states in this manner. This difference between J- and K-changing collisions was observed for both $^{13}CH_3F$ and $^{12}CH_3F$. A computer program based on this model for rotational energy transfer (RET) shows that all rotational collisional processes observed in CH_3F can be modeled with only four free parameters—one for dipole–dipole collisions, two for either the SPG or IOS-P law, and a cumulative rate for K-changing collisions.[6]

Using time-resolved IRMMDR, we have studied both rotational and vibrational collision processes in CH_3Cl. However, the present paper is limited to the discussion of rotational processes; the results concerning vibrational processes will be reported later. In early work on CH_3Cl using a similar experimental technique, but not resolved in time and using a limited range of probe frequencies, Frenkel *et al.* found that $|\Delta J|=1$ is more common than $|\Delta J|>1$ in $\Delta K=0$ collisions, but that in $\Delta K=-3$ collisions, large changes in J were relatively more common.[9] These findings are consistent with the more detailed descriptions of RET in the CH_3F studies of Everitt and De Lucia.[5,6] The purpose of the present study is to characterize the rotational and vibrational collisional processes of CH_3Cl and model them with a few parameters, and where possible, relate these parameters to those of CH_3F and fundamental molecular processes. This objective has been achieved for the wide range of states pumped and probed in this experiment. We report here that

[a]Department of Physics, The Ohio State University, Columbus, Ohio 43210.
[b]Army Research Office, Physics Division, Research Triangle Park, North Carolina 27709.

 0021-9606/94/100(8)/5666/18/$6.00

J-changing collisions in CH_3Cl (for $v_6=1$ of CH_3Cl, $\Delta J=n$, $\Delta K=0$, $\Delta l=0$, where n is an integer and l is the quantum number for angular momentum from the degenerate v_6 vibrational motion) are very similar to those in CH_3F. However, a difference between the experimental observations of CH_3Cl and CH_3F led to a generalization of the model for thermal K-changing collisions (for $v_6=1$ of CH_3Cl, $\Delta J=m$, $\Delta(K-l)=3n$, where m and n are integers and l is the same as above) that uses a small number of parameters, all of which are physically meaningful.

Other RET studies using a variety of experimental techniques have been performed on CH_3F. Oka laid out the basic propensity rules for RET in symmetric top molecules such as CH_3F as well as other molecules in his pioneering microwave double resonance experiments.[8] In free-jet expansion experiments, Douketis and co-workers found that the J degree of rotational freedom of CH_3F in collisions with He cools twice as effectively as that of K.[10] Schwendeman and co-workers have studied CH_3F in a series of frequency-resolved infrared–infrared double resonance experiments (IRIRDR) observing collisional processes in addition to collisionless effects.[11–15]

Several experimental techniques have been used to study RET in many other molecules with a variety of collision partners. A large body of experimental and theoretical work with diatomic molecules has established scaling laws that accurately describe RET using a small number of parameters.[16–23] The rates of J-changing RET in some early studies of dipolar molecules [NH_3,[24] CDF_3,[25] and CH_3F (Ref. 11)] were explained using only $\Delta J=\pm1$ and possibly $\Delta J=\pm2$ collisions; however, recent studies have shown that large changes in the J quantum number can occur in single collisions and can contribute significantly to RET measurements.[6,26–29] In fact, the need to include higher-order moments ($|\Delta J|\geq2$) in NH_3 was suggested as early as 1974.[30] Orr and co-workers found J-changing collisions in D_2CO are modeled well by either the exponential energy gap law (EGL) or the SPG law, but that a series of $\Delta J=\pm1$ and $\Delta J=\pm2$ collisions alone was unable to reproduce their measurements.[26,31,32] Measurements of state-to-state rates in self-collisions of C_2H_2 have shown significant rates for large changes of J.[33] Steinfeld and co-workers reported that J-changing collisions in NH_3 can also be modeled by the EGL fitting law.[29] Furthermore, a theoretical treatment by Parson[34,35] showed that on the time scale of collisions, two spherical top molecules studied by the Steinfeld group, $^{13}CD_4$ (Refs. 27 and 36) and SiH_4 (Ref. 28) can be treated as symmetric tops as a result of temporary rotational distortion around a threefold or a fourfold symmetry axis. This physical effect results in "principal channels" for RET in spherical tops similar to J-changing RET in symmetric tops. Hetzler and Steinfeld showed that RET in these principal channels can also be modeled by the EGL fitting law with changes of J up to $|\Delta J|=5$ observed for SiH_4.[28] As mentioned above, Everitt and De Lucia showed that both the SPG and IOS-P laws accurately model J-changing collisions in CH_3F.[6]

There have also been a limited number of experimental studies of K-changing rotational collisions in nonlinear molecules, all of which corroborate the strength of Oka's symmetry preservation rule $\Delta K=mn$, where m is the order of the symmetry axis and n is an integer.[8] The study of Frenkel *et al.* gave an early indication that K-changing collisions in CH_3Cl can change J by several quantum numbers.[9] Several years later in reports based on time-resolved measurements of a large number of states, De Lucia and co-workers reported that the $\Delta K=3n$ process in CH_3F is thermal with a cross section larger than the gas kinetic collision cross section.[4,5] The presence of a $\Delta K=3n$ process in CH_3F has been confirmed by Shin *et al.* in their frequency domain IR-IRDR measurements.[12] Harradine *et al.* have also observed K-changing collisions of at least $\Delta K=-15$ in self-collisions of CDF_3.[25] However, their results do not indicate that the K-changing process in this oblate top is thermal in both J and K since they found that only a narrow distribution of J states is populated by K-changing collisions. Orr and co-workers have also discussed K_a-changing collisions in the asymmetric top D_2CO.[31] In a paper concerned primarily with J-changing collision rates, they modeled population loss into states of different K as occurring with the gas kinetic collision rate for only $\Delta K_a=\pm2$ and $|\Delta E|<10\ cm^{-1}$, while all other K-changing state-to-state rates were zero. Large changes of J were required to meet the limited-energy-change requirement. However, in more recent work, they have used a different model that allows large changes of K, $\Delta K_a=\pm2n$ to conserve symmetry, but only zero or small changes of J for collisions that change K.[32] Although a detailed report of K-changing collisions in D_2CO has not been published, it appears that the $\Delta K_a=\pm2n$ process is not thermal in this near-prolate top; however, large changes of K do occur. Abel *et al.* have reported state-to-state rates for K-changing collisions in NH_3 self-collisions and in collisions with Ar.[29] For self-collisions, a comparison of J-specific $\Delta K=-3$ collision rates with $\Delta K=0$ collision rates shows that the K-changing collisions are less probable and their rates vary more slowly in J. This would be expected since they involve higher-order moments of the intermolecular potential. Abel *et al.* obtained reasonable fits to the individually measured state-to-state rate constants by modeling the $\Delta K=-3$ collisions using the energy corrected sudden (ECS) law and basis rates that vary slowly in multipole order. Thus for another molecule, K-changing collisions have been shown to be less state selective than J-changing collisions; however, the K-changing collisional process in NH_3 is again not thermal as in CH_3F and CH_3Cl.

II. BACKGROUND

This work builds on an understanding of the collisional processes of CH_3F.[3,5,6,11,37] The expectation was that CH_3Cl would exhibit the same basic collisional processes as CH_3F, although perhaps with different rates. Since the CH_3Cl model is a generalized version of the CH_3F model, the CH_3F work is reviewed in the following section. As well as defining the basic components of the model, this section also provides a framework for comparing the rotational processes of CH_3F and CH_3Cl.

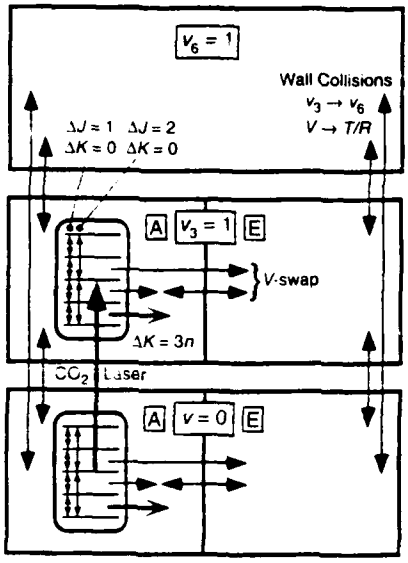

FIG. 1. The RET model used for CH_3F (Refs. 5 and 6). Only the ground vibrational states $v_3=1$ and $v_6=1$ (the lowest energy vibrational modes) needed to be included to accurately model the IRMMDR time responses for pump intensities that were used. Examples of the measured collisional processes are denoted with arrows. While only two types of J-changing, $\Delta K=0$ processes are drawn, they were all modeled using a scaling law.

A. J-changing collisions

The action of the pump in this double resonance experiment is to populate a single rotational level within an excited vibrational state with molecules from a single rotational state of the ground vibrational state. Figure 1 shows this schematically for $^{13}CH_3F$. In the earlier Duke Microwave Laboratory work,[1-6] two coincidences with $^{12}C^{16}O_2$ laser lines were used extensively—$9P(32)$ pumps $^{13}CH_3F$ population from $J=4$, $K=3$ of the ground vibrational state to $v_3=1$, $J=5$, $K=3$, and $9P(20)$ pumps $^{12}CH_3F$ population from $J=12$, $K=2$ of the ground vibrational state to $v_3=1$, $J=12$, $K=2$. As the pump introduces excess population in the excited vibrational state, several collisional processes reestablish rotational thermal equilibrium within $v_3=1$. Likewise, several vibrational collisional processes operate on longer time scales to equilibrate population among the vibrational levels.

The fastest of the collisional mechanisms is the dipole–dipole process. The well-known selection rules for this process are $\Delta J=0,\pm1$, $\Delta K=0$, where the branching ratios are given by the dipole matrix elements for a symmetric top[38]

$$k_{J\rightarrow J+1}=k_{dd}\frac{(J+1)^2-K^2}{(J+1)(2J+1)},$$
$$k_{J\rightarrow J}=k_{dd}\frac{K^2}{J(J+1)}, \tag{1}$$

and

$$k_{J\rightarrow J-1}=k_{dd}\frac{J^2-K^2}{J(2J+1)},$$

where k_{dd} is the dipole–dipole collision rate and the matrix elements have been summed over M. In addition, a detailed balance factor is included for transitions downward in energy.

Higher-order collision processes that change the J state by several quanta in a single collision, up to $\Delta J=-10$, while leaving K unchanged were also observed in CH_3F.[6] These collisions are characterized by selection rules $\Delta J=n$, $\Delta K=0$, where n is determined by the orders of the interacting multipole moments.[8] Examples of the $\Delta J=2$ process are shown in Fig. 1. Since they can populate states several J quantum numbers away from the pumped state in a single collision, the effects of these higher-order collisions are easy to observe several J away from the pumped state despite having smaller cross sections than the dipole–dipole process; in fact, they are essential for reproducing the observed population flow of the CH_3F system. Multiple dipole–dipole collisions alone are not sufficient to account for the observed IRMMDR time responses of states several J away from the pumped state.[6] This is because the pseudorandom walk of the dipole–dipole process in this one dimensional system requires on the order of n^2 collisions to move population n steps in J, whereas the appropriate higher-order process requires only one collision to change J by the same number.

It has been shown that both the infinite order sudden scaling law (IOS) and the statistical power gap fitting law (SPG) successfully quantify the observed J-changing rate constants in CH_3F.[6] The IOS equation for $\Delta J=n$, $\Delta K=0$ collisions in CH_3F is[16]

$$k_{J_i\rightarrow J_f}=(2J_f+1)\exp\left(\frac{E_J-E_{J_>}}{kT}\right)\sum_{L=|J_i-J_f|}^{J_i+J_f}(2L+1)\times\begin{pmatrix}J_i & J_f & L\\ -K & K & 0\end{pmatrix}^2 k_{L\rightarrow0}, \tag{2}$$

where $(:::)$ is a 3-J symbol and the exponential factor accounts for detailed balance, $J_>$ being the greater of J_i and J_f. The basis rates, which could be derived if the intermolecular potential were known, were assumed to have the power law form $k_{L\rightarrow0}=c[L(L+1)]^{-\gamma}$ (thus abbreviated IOS-P). The statistical power gap law, which Smith and Pritchard showed to be an analytical approximation of the IOS-P scaling law,[22] was calculated using

$$k_{J_i\rightarrow J_f}=c(2J_f+1)\exp\left(\frac{E_J-E_{J_>}}{kT}\right)\left|\frac{\Delta E}{kT}\right|^{-(2\gamma-1)}. \tag{3}$$

This is a limiting case of the SPG law valid in the regime where $|\Delta J|/(J_i+J_f)$ and $|\Delta E|/kT$ are small compared to 1; both are true for the measurements of CH_3F.

B. K-changing collisions

Before discussing K-changing collisions, we would like to clarify our use of the word *thermal*. In this paper, thermal is used to describe both state population distributions and collisional processes. By *thermal group of states*, we mean that the population within these states can be described by a Boltzmann distribution with a single, not necessarily ambi-

ent, temperature. Note that there may be a number of different thermal groups and that the total population in a group is not fixed to any specific value and may even vary with time. In addition, the temperature may vary with time, but eventually both the temperature and the total population of the group relax to their final, ambient values. Often, we refer to a thermal group of states as a *pool* of states. The experimentally determined existence of thermal pools significantly simplifies the modeling of population flow since, for each thermal group, the population in a large number of states can be described by just two variables. For example, since rotational processes are generally faster than vibrational processes, the population of rotational states within a given vibrational state often reaches a Boltzmann distribution (i.e., becomes thermal) before the population distribution among the different vibrational levels reaches equilibrium. As another example for a symmetric top, the rotational states of the same vibrational energy and symmetry as the pumped state may become thermal as a group and still not be in thermal equilibrium with the states of the other symmetry type, even though they too are thermal as a group.

By *thermal process*, we mean that the state-to-state rates to all of the eligible final states (states satisfying the selection rules of the process) are such that the population transferred into these final states is distributed according to a Boltzmann distribution with a single temperature. As is the case for the temperature of the thermal pools, the temperature for the thermal process may or may not be the same as the temperature of the cell. Similar to the thermal pool concept, the motivation for modeling processes as thermal is to represent many individual state-to-state rates with only a net rate and a temperature. Since concepts of thermal pools and rates are justified by the data, we use them to greatly simplify the description of the RET processes, thereby yielding a rigorous, yet tractable, model.

In addition to the J-changing processes discussed above, K-changing collisions also rapidly depopulate the pumped state. It is well documented that because of nuclear spin statistics, changes in K for a symmetric top molecule with C_{3v} symmetry are restricted to multiples of three on the time scales of experiments such as this.[8] Note that since the $\pm K$ levels are degenerate, all of the $K \neq 3n$ states are coupled by these collisions (e.g., $K=1 \rightarrow -2$). Both CH_3F and CH_3Cl fall into this symmetry class. Everitt and De Lucia showed the $\Delta K = 3n$ process in CH_3F has the remarkable characteristic of being thermal.[5] For CH_3F, a Boltzmann distribution at the ambient temperature of the cell (300 K) adequately represented the distribution of the $\Delta K = 3n$ final states. This characteristic was tested by measuring many different rotational states for two different pump coincidences for two different isotopic species, $^{12}CH_3F$ and $^{13}CH_3F$. As will be discussed later, our millimeter–submillimeter wave (mm/submm) probe is highly sensitive to rotational nonequilibria, so the experimental evidence is compelling that the states that receive population through the $K = 3n$ process maintain a thermal distribution of population. K-changing RET in CH_3F does not show any state specificity beyond the following requirements: the vibrational state does not change; the symmetry type does not change; and the amount of population a state receives is proportional to its contribution to the rotational partition function. This last requirement is in sharp contrast to the dipole–dipole and the higher-order J-changing collisional processes which are distinguished by J selection rules.

The thermal K-changing process greatly reduces the complexity of the description of the CH_3F system. Without such a process, the N thermally accessible states in $v_3=1$ might be connected by up to $N(N-1)/2$ separate rates. Instead, the existence of the thermal $\Delta K = 3n$ process allows all of the rotational states of different K than the pumped state to be grouped into two pools—the pool of E symmetry states and the pool of A symmetry states.

As Everitt pointed out,[37] it is not clear that the temperature of the distribution of $\Delta K = 3n$ final states should necessarily be the same as the ambient temperature of the gas as was reported for CH_3F.[5] Based on an energy conservation argument, it might be expected that the temperature of the distribution of final states should be different from the cell temperature since the rotational energy of the pumped state is in general different than E_{kT}. This will be shown to be the case for CH_3Cl.

C. Vibrational state-changing collisions

The previous work showed that for CH_3F, some vibrational processes operate on nearly the same time scale as the rotational processes; therefore, they cannot be ignored when analyzing experimental RET data.[5] However, since the focus of this paper is restricted to the rotational processes, we will discuss the vibrational processes only insofar as necessary to deal quantitatively with the rotational collisional mechanisms. The vibrational processes in CH_3Cl have been measured and will be treated further in a future paper.

The fastest vibrational process in CH_3F is the near-resonant vibrational swap (V-swap) mechanism

$$CH_3F(v_3=1)_A + CH_3F(v=0)_B \rightarrow CH_3F(v=0)_A + CH_3F(v_3=1)_B - \Delta E, \quad (4)$$

where the two molecules labeled A and B each retain their symmetry. Here the vibrationally excited molecule A exchanges a unit of vibrational energy with a ground state molecule B. If the colliding molecules are of opposite symmetry, this has the effect of transcending the symmetry selection rule. The rate for this process in CH_3F is not much less than the rates of the rotational processes.[5,7]

D. Wall collisions

For the cell size and gas pressures we typically use, the most important mechanism for relaxing the fundamental vibrational quantum is wall collisions. The previous CH_3F analysis, performed using a 2 cm diameter copper tube, showed that a wall collision has a high probability for thermalizing a molecule's vibrational energy.[4] At pressures low enough that the mean free path becomes long compared to the radius of the cell, most molecules that are excited by the pump move to the wall without undergoing any velocity-changing collisions. (Note that we can still observe collision induced IRMMDR time responses at these low pressures

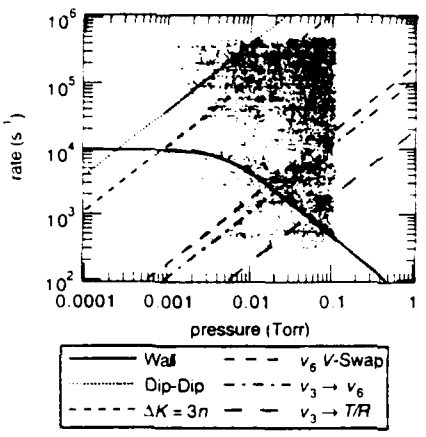

FIG. 2. CH_3Cl collision rates vs pressure. The region between 1 and 100 mTorr is the pressure range for the measured rotational collision data. Note that the molecules' motion to the wall changes from ballistic to diffusive at a pressure of about 5 mTorr for the cell of 4.82 cm diameter.

since many of the state-to-state rates of rotational processes are faster than the gas kinetic collision rate.) Diffusion begins to dominate the motion to the wall starting at a pressure of roughly 10 mTorr for room temperature CH_3F in a 2 cm diameter cell. While the rate of diffusion to the wall is inversely proportional to pressure, the rates for the two-body collisional processes we study are linear in pressure; consequently, it is easy to distinguish relaxation at the wall from molecule–molecule relaxation processes by acquiring data over an appropriate range of pressures. Figure 2 shows the pressure dependence for CH_3Cl processes in a 4.82 cm diameter cell used in the present experiment.

III. EXPERIMENT

Although the experimental setup is similar to that reported previously,[4-6] the apparatus will be presented here to provide a description of recent experimental enhancements. Figure 3 shows the essential elements of this experiment. A Q-switched CO_2 laser coincidence with a CH_3Cl infrared transition provides a nonthermal population distribution in a particular rotational state of the $v_6=1$ vibrational state of

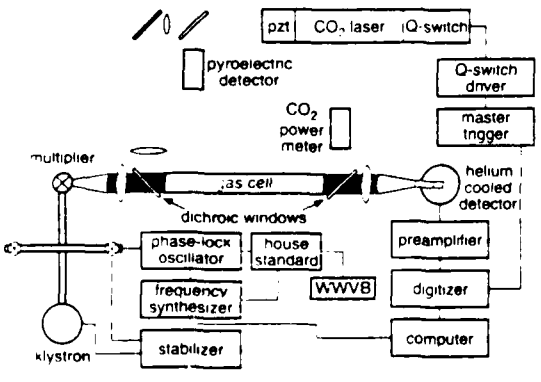

FIG. 3. Block diagram of the time-resolved IRMMDR experiment.

CH_3Cl. A mm/submm spectrometer simultaneously probes a single rotational transition within the excited vibrational state. The time-resolved measurements include both three-level double resonances, where the pumped state is also one of the probed states, and collisionally mediated four-level measurements. Using a model of the collisional processes and the measured time-varying absorption (or emission) signals, a nonlinear least squares routine then fits the rates of the population flow processes.

For this CH_3Cl study, a higher power infrared source was used. The CO_2 laser is a 50 W Apollo model 570 longitudinal gas flow laser that we modified to enable Q switching by the addition of an intracavity CdTe electro-optic modulator. This system allows pulse widths to be adjusted to as narrow as 0.5 μs full width at half-maximum (FWHM). Average powers per pulse of over 400 W are produced for the $9P(26)$ laser line at a 1 kHz repetition rate. The diffraction grating that provides single line oscillation, while allowing full coverage of both the 9 and 10 μm bands of $^{12}C^{16}O_2$ is mounted on a piezoelectric translation stage to allow fine tuning of the laser cavity.

The mm/submm radiation is generated using harmonic generation techniques developed in the Duke Microwave Laboratory by King and Gordy[39] and extended to the 1 THz range by Helminger, Messer, and De Lucia.[40,41] A phase stabilized 35 GHz klystron is impedance matched onto a point-contact diode, which generates radiation at integer multiples of the klystron frequency. The desired harmonic is selected by varying the size of the multiplier's output waveguide and by tuning the impedance matching at the diode. Interchanging klystrons and output frequency cutoffs allows continuous coverage of the mm/submm spectrum from less than 100 GHz to greater than 1 THz. The phase-lock system used in this experiment yields a fractional linewidth of better than 10^{-7} and a frequency accuracy of better than 10^{-8}.

The body of the diagnostic cell used for obtaining the CH_3Cl data is a stainless steel pipe 1.0 m long by 4.82 cm diameter. The larger diameter of this new cell increases the time for molecules to reach the cell wall and thus allows measurements to be made at lower pressures where collisional rates are slower. End pieces housing dichroic windows were used to reflect the CO_2 laser radiation and to transmit the mm/submm waves. The radii of both the pump and probe beams are expanded to about 80% of the cross sectional radius of the cell. After the beams copropagate the full length of the cell along its axis, the second dichroic window splits the beams; the laser power that is not absorbed by the gas is monitored at a Scientech 362 power meter, while the mm/submm radiation is directed to the spectrometer's broadband detector. The measurements reported here were made at pressures of 1–1000 mTorr and at room temperature.

A significant improvement to the experiment over that used in previous papers from this laboratory is the ability to distribute both pump and probe radiation smoothly over the cross section of the diagnostic cell. This is achieved by using large aperture dichroic windows to combine the radiation rather than the former scheme where the laser beam was focused through a pinhole in the cell wall. The dichroic windows were fabricated of a multilayer coating of Ge and ZnS

on a low-water fused silica substrate. At the 45° incidence used in the experiment, the windows have a reflectivity of greater than 92% across the 9 μm band of the CO_2 laser and 94.3% at the 9.6 μm $9P(26)$ line. The laser power that is not reflected at the dichroic's coated surface is absorbed by the substrate; the spectrometer's broadband detector did not measure spurious laser radiation. We measured these windows to be no worse than 75% transmissive to both 150 and 300 GHz radiation at 45° incidence.

The mm/submm detector is an InSb hot electron bolometer operated at the He-cooled temperature of about 1.7 K. The detector bandwidth is about 1 MHz. Improved signal averaging is now provided by two computer-aided measurement and control (CAMAC) modules, the dsp Technologies 2030S transient digitizer, and 4101 averaging memory. This system captures every waveform at the typical repetition rate of 1 kHz. In most cases, 60 000 waveforms were summed for a total integration time of 1 min. Most of the signals were averaged over a 100 μs window at a digitization rate of 0.133 μs; however, a 300 μs window and 0.333 μs rate were used for the slowest IRMMDR time responses.

Time-resolved IRMMDR is particularly well-suited for studying rovibrational collisional kinetics because of the sensitivity of the mm/submm rotational absorption (and emission) measurements, particularly to nonthermal rotational population distributions. While the experiment is sufficiently sensitive to measure time responses for states populated thermally (with a signal to noise ratio of better than 10:1 for 1 MHz bandwidth and 60 s integration for many pump-symmetry transitions), the experiment is much more sensitive to states populated nonthermally. The large nonthermal signals are in some cases due to the large pump-induced deviations of the rotational populations from thermal distributions. In addition, rotational absorption probing of this region of the spectrum is intrinsically very sensitive to even small deviations from thermal population distributions. This sensitivity is crucial to the verification of the thermal nature of some of the collisional processes. The sensitivity to nonthermal deviations is illustrated by the following example: at 212 GHz, there is only a 3.4% thermal population difference between probed rotational states, and this difference produces the easily observed absorption of 0.5% in the excited vibrational state (even though rotational states in the $v_6=1$ vibrational state have only 1/140 as much population as those in the ground vibrational state). Therefore, if the population of one state deviates from thermal by a factor of only 0.1%, then the absorption will change by 0.015%, which results in a signal to noise of about 5:1 for our typical time-resolved bandwidth of 1 MHz and 60 s integration.

IV. SPECTROSCOPIC CONSIDERATIONS

Table I contains the pump and probe transitions used in this work. The IRMMDR time responses used for fitting the collision rates were taken when the laser was tuned to maximum power and the mm/submm probe was tuned to the line center; however, many other time responses were acquired with the pump, probe, or both offset in frequency. The isotopic species of CH_3Cl were present in natural abundances 76% ^{35}Cl and 24% ^{37}Cl. For the large part, we both pumped and probed $CH_3{}^{35}Cl$; however, we did spot check all three other permutations—pump $CH_3{}^{35}Cl$, probe $CH_3{}^{37}Cl$; pump $CH_3{}^{37}Cl$, probe $CH_3{}^{35}Cl$; and pump $CH_3{}^{37}Cl$, probe $CH_3{}^{37}Cl$. A description of the isotopic species study will be reported in a future paper. In contrast to those used with CH_3F, none of the CO_2–CH_3Cl coincidences used in this study displayed any behavior indicating multiple coincidences for a given pump line. For $^{12}CH_3F$, the $9P(20)$ pump line put small populations in $K=1$ and $K=0$ of $J=11$ in addition to the main pumped state $J=11$, $K=2$.

Several spectroscopic circumstances conspire to make this CH_3Cl study more challenging than that of the CH_3F work, two of these being methyl chloride's hyperfine structure and l-type doubling in its pumped vibrational state. Figure 4 shows the rotational energy levels of $v_6=1$ for CH_3Cl. Chlorine's large quadrupole moment causes hyperfine splitting that is resolved over most of our working pressure range, making the CH_3Cl spectrum dense. In addition, l-type doubling is an issue in the CH_3Cl work because the CO_2 laser coincidences with CH_3Cl involve transitions from the ground state to the doubly degenerate $v_6=1$ bending state. K is the total angular momentum about the molecular symmetry axis consisting of pure rotational angular momentum K' and a contribution from the vibrational motion l. The overall symmetry of a rotational state is determined by $K'=K-l$, where A symmetry states consist of those with K' equal to a multiple of three and the E symmetry states consist of the remaining states. The symmetry preservation propensity rule that applies to RET in the l-type doubled $v_6=1$ vibrational manifold of CH_3Cl is $\Delta(K-l)=3n$, where n is an integer.

Both hyperfine structure and l-type doubling increases the density of the CH_3Cl rotational spectrum compared to the spectrum for $v_3=1$ in CH_3F. The hyperfine structure also reduces the absorption coefficients of the resolved lines. The weaker pump and probe absorption coefficients for $v_6=1$ of CH_3Cl made necessary many of the experimental improvements mentioned above. Although hyperfine structure and l-type doubling contribute to the complexity of the CH_3Cl spectrum, they also provided additional rotational states to probe and, therefore, the possibility of gaining additional information about the rotational collision processes.

Another significant difference with CH_3F is that CH_3Cl has a convenient CO_2 pump coincidence that populates a state with rotational energy greater than room temperature thermal energy. The CH_3F pump lines used in the earlier study correspond to energies of 64 cm^{-1} for the $9P(32)$ coincidence with $^{13}CH_3F$ and to 148 cm^{-1} for $9P(20)$ with $^{12}CH_3F$, both of which are below the 205 cm^{-1} room temperature thermal energy. In contrast, the CH_3Cl pump coincidences are 85 cm^{-1} for $9P(26)$ and 285 cm^{-1} for $9R(12)$. As will be discussed below, the energy difference between the pumped states in CH_3Cl aided in the analysis of its collision processes.

V. EXPERIMENTAL RESULTS

A. Explanation of IRMMDR time response data

Based on experimental measurements, the IRMMDR time responses of the transitions we measured may be

TABLE I. Pump and probe transitions used in the IRMMDR measurements of $CH_3{}^{35}Cl$.

Pump coincidences

CO_2 line	Frequency (cm^{-1})	Ground state J	Ground state K	$v_6=1$ J	$v_6=1$ K	$v_6=1$ l	Frequency offset (MHz)
$9R(12)$	1073.278	11	6	12	7	1	−30
$9P(26)$	1041.280	5	3	6	4	1	20

Probe Transitions

Transition Vib	Transition $J\rightarrow J'$	Transition K	Transition l	Symmetry	Frequency[a] (GHz)
$v_6=1$	3-4	−1	−1	A	105.8915
$v_6=1$	3-4	1	1	A	106.0079
$v_6=1$	3-4	2	−1	A	105.9353
$v_6=1$	4-5	−1	−1	A	132.3594
$v_6=1$	4-5	1	1	A	132.5051
$v_6=1$	4-5	2	−1	A	132.4103
$v_6=1$	4-5	4	1	A	132.4213
$v_6=1$	5-6	−1	−1	A	158.8268
$v_6=1$	5-6	1	1	A	159.0016
$v_6=1$	5-6	2	−1	A	158.8910
$v_6=1$	5-6	4	1	A	158.8977
$v_6=1$	5-6	5	−1	A	158.8130
$v_6=1$	6-7	−1	−1	A	185.2913
$v_6=1$	6-7	1	1	A	185.4952
$v_6=1$	6-7	2	−1	A	185.3643
$v_6=1$	6-7	4	1	A	185.3725
$v_6=1$	6-7	5	−1	A	185.2888
$v_6=1$	7-8	−1	−1	A	211.7528
$v_6=1$	7-8	1	1	A	211.9857
$v_6=1$	7-8	2	−1	A	211.8366
$v_6=1$	7-8	4	1	A	211.8448
$v_6=1$	7-8	5	−1	A	211.7428
$v_6=1$	7-8	7	1	A	211.7660
$v_6=1$	8-9	−1	−1	A	238.2109
$v_6=1$	8-9	1	1	A	238.4728
$v_6=1$	8-9	2	−1	A	238.3055
$v_6=1$	8-9	2	1	E	238.3399
$v_6=1$	8-9	3	−1	E	238.2788
$v_6=1$	8-9	4	−1	E	238.2447
$v_6=1$	8-9	4	1	A	238.3137
$v_6=1$	8-9	5	−1	A	238.2018
$v_6=1$	8-9	6	−1	E	238.1553
$v_6=1$	8-9	7	1	A	238.2213
$v_6=1$	9-10	2	−1	A	264.7700
$v_6=1$	9-10	4	1	A	264.7787
$v_6=1$	10-11	2	−1	A	291.2302
$v_6=1$	10-11	4	1	A	291.2396
$v_3=1$	4-5	3		A	131.7527
$v_3=1$	8-9	0		A	237.1448
$v_3=1$	8-9	1		E	237.1412
$v_3=1$	8-9	2		E	237.1305
$v_3=1$	8-9	3		A	237.1124
$v_3=1$	8-9	4		E	237.0876

[a]Here hyperfine components are resolved at 20 mTorr, the rotational frequencies were chosen to minimize spurious signals from nearby transitions.

grouped into two categories—those where the states involved in the transition have a nonthermal population distribution and those involving states that maintain a thermal population distribution.

Nonthermal. For the first several microseconds following the pump pulse, the transitions involving states of the same K and l as the pumped state displayed strong nonequilibria due to the fast dipole–dipole and other significant multipole–multipole collisional processes. (We refer to a set of J states with the same K and l and within the same vibrational state as a "K/l stack.") The signal to noise estimation in the Experiment section above shows the high sensitivity to these nonthermal IRMMDR time responses in the pumped K/l stack.

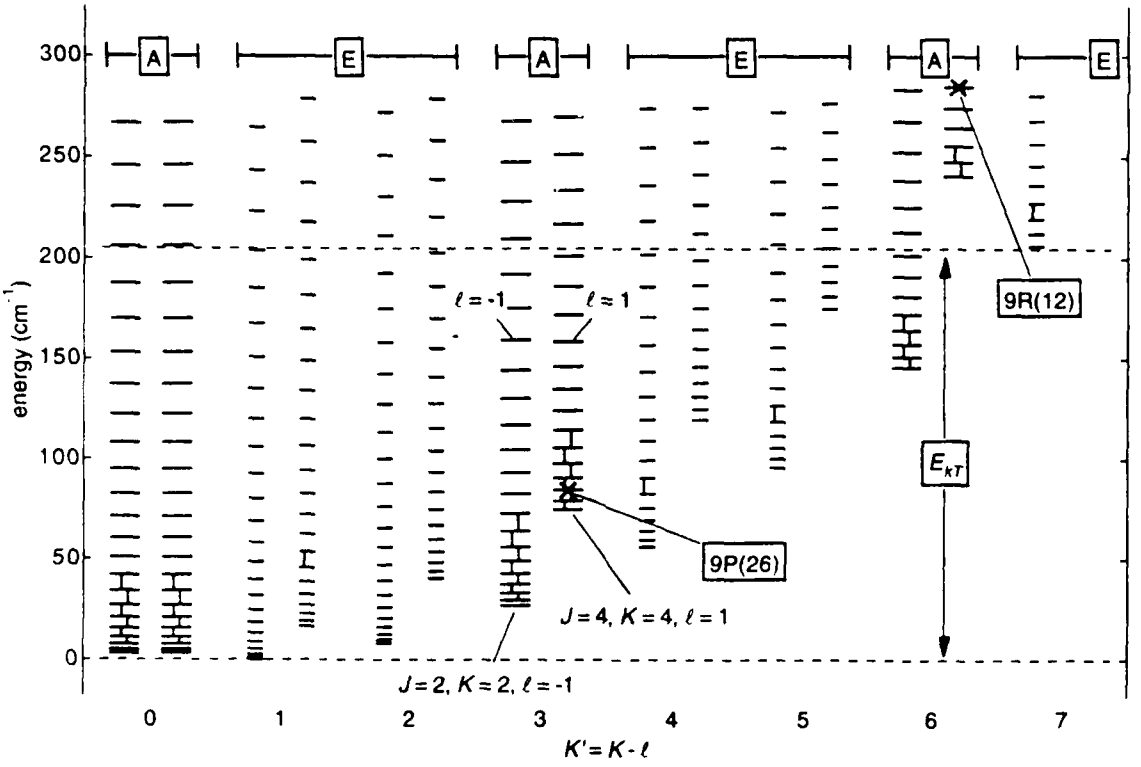

FIG. 4. Rotational energy levels of the $CH_3{}^{35}Cl$ $v_6 = 1$ vibrational manifold, which experiences l-type doubling. Hyperfine components of a state have been reduced to a single value by taking a weighted average. K/l stacks are paired by K' with the $l = -1$ stack on the left and the $l = 1$ stack on the right. The two states that are populated by the CO_2 pump are labeled $9P(26)$ and $9R(12)$. Transitions for which we have acquired IRMMDR time responses are marked with vertical lines. The A symmetry states, the pump symmetry for both coincidences, are shown wider than the E symmetry states.

Thermal. Time responses involving all other $v_6 = 1$ states belonged to one of two thermal pools—the A symmetry pool and the E symmetry pool. As stated before, all states within a pool remain in thermal equilibrium among themselves, even though both the temperature and total population of the pool are free to change in time. However, if the pool temperature remains fixed at the temperature of the cell, then all of the time responses of a pool have the same amplitude-normalized shape as was observed in CH_3F.[5]

The probe monitors a difference in population between two adjacent J states. We checked for M selectivity in the observed time responses involving the pumped state by making measurements with the linear pump and probe polarizations parallel and perpendicular to each other; however, we did not observe any systematic difference in the time responses as has been observed in H_2CO.[42] Consequently, the model assumes all M levels are populated equally. For our IRMMDR data, the zero absorption level of a time response corresponds to an ambient equilibrium population difference between the two states; consequently, absorption measurements are relative to the signal from the thermal "background" population since the pump does not significantly heat the gas. If the population difference between the lower and upper states decreases, the detector measures a negative signal which corresponds to the decreased absorption (more probe power arrives at the detector). However, since we are concerned with the population differences that deviate from

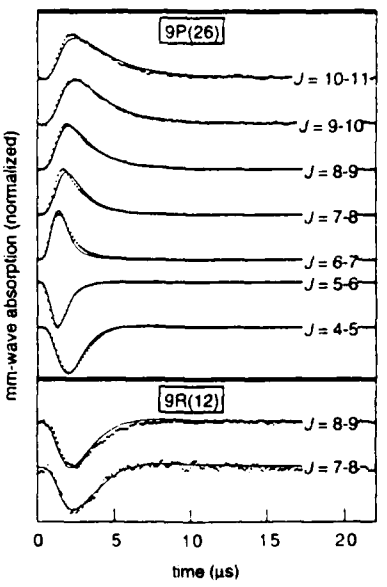

FIG. 5. IRMMDR time responses of several transitions in the pumped K/l stack. The state populated by the $9P(26)$ line is $J = 6$, $K = 4$, $l = 1$ and the state populated by the $9R(12)$ line is $J = 12$, $K = 7$, $l = 1$. The data (dots) were taken at 20 mTorr. The fits for both pump coincidences (solid lines) were performed simultaneously for these time responses and 44 others at different pressures using the IOS-P scaling law for all $\Delta K = 0$ collisions.

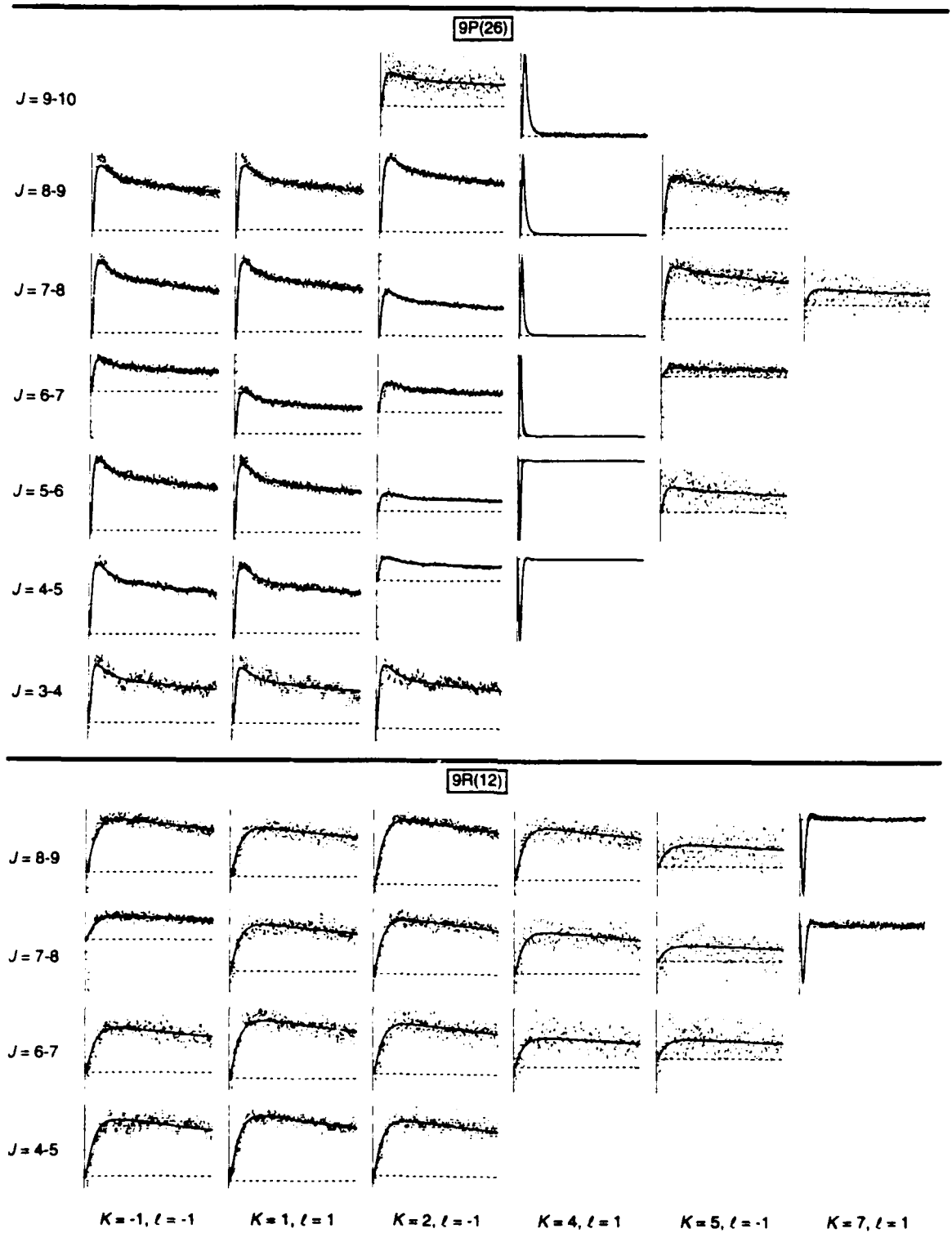

FIG. 6. Measured CH_3Cl $v_6=1$, A symmetry IRMMDR time responses for several rotational states at 30 mTorr with fit time responses for two different pump lines, $9P(26)$ and $9R(12)$. Each vertical axis is the normalized millimeter-wave absorption and each horizontal time axis covers 60 μs. The graphs are arranged in the same order as the A symmetry energy levels shown in Fig. 4. The dots are the data, the solid lines are the fit time responses, and the dashed lines indicate the equilibrium absorption levels. For $9P(26)$, the pumped K/l stack is $K=4$, $l=1$ and for $9R(12)$, it is $K=7$, $l=1$. The fitted time responses for J-changing collisions were modeled using the IOS-P model.

the equilibrium distribution, we refer to any decreased absorption as emission, even though the net effect may just be reduced absorption. Furthermore, since the thermal background population is approximately constant in time, only the pumped molecules undergo state-changing collisions in the model. Accordingly, the thermal background population is not included in the definitions of the pools for modeling purposes, and when we refer to the Boltzmann distribution of

population in a pool, it is only the pumped molecules that have not yet been vibrationally thermalized that we consider.

B. A comparison with CH_3F

As expected, there were many similarities between the experimental results for CH_3F and CH_3Cl. There were several types of IRMMDR time responses in both molecules—nonthermal time responses for J-changing collisions, and the time responses of several thermal pools. However, the time responses for CH_3Cl states populated by K-changing collisions showed some significant differences from the CH_3F data.

Figure 5 shows the IRMMDR time responses of several transitions in the pumped K/l stacks of CH_3Cl. The behavior of these states is very similar to those of the pumped K stack in CH_3F. The largest and fastest IRMMDR time responses come from the three-level double resonance measurements. Time responses in the same K/l stack as the pumped state become increasingly smaller and slower with increasing $|\Delta J|$. For the $9R(12)$ pump, all of the measured transitions in the pumped K/l stack were below the $J=12$ pumped state; consequently, all exhibited emission.

The IRMMDR time responses for CH_3Cl states populated by vibrational processes are also similar to those of CH_3F; however, the v_6, V-swap process in CH_3Cl is slower than the v_3, V-swap process in CH_3F. This is due to the smaller transition moment for bending mode transitions in $v_6=1$ of CH_3Cl.[43,44] Additionally, the $v_3=1$ states are populated by the *nonresonant* $v_3 \leftrightarrow v_6$ *vibrational process*, and the $V \rightarrow T/R$ process is an important vibrational relaxation process at higher pressures where the diffusion rate to the wall is slower.

While the IRMMDR time responses of the above CH_3Cl transitions are very similar to those of CH_3F, the time responses of the states populated by K-changing collisions (i.e., the $v_6=1$, A states) are different. Figure 6 shows a number of CH_3Cl time responses for the $v_6=1$, A states using both pump lines. Similar data were acquired for other pressures from 1 to 100 mTorr. The following are some of the salient features of these time responses: (1) *K-changing collisions are fast.* As was the case in CH_3F, K-changing collisions occur at a rate comparable to gas kinetic collisions. Furthermore, the cumulative rate for K-changing collisions is within an order of magnitude of the rate of the dipole–dipole process. (2) *IRMMDR time responses are different for the 9P(26) and 9R(12) pump lines.* As seen in $9R(12)$ time responses of Fig. 6, the measurements with the $9R(12)$ pump coincidence are similar to those of CH_3F, in that all of the time responses have the same shape to within the noise level. However, the measurements made using the $9P(26)$ pump line reveal an additional early time feature (ETF) that was not observed in the CH_3F data. An ETF is the fast rise and fall seen in a $9P(26)$ time response at early time, especially at lower K', that is absent in the same transition when using the $9R(12)$ pump line. (3) *IRMMDR time responses are thermal in J.* This is true for the data of both pump coincidences. The sharp nonthermal features found in the pumped K/l stack data of Fig. 6 are not present in the time responses of the transitions that are populated by K-changing collisions.

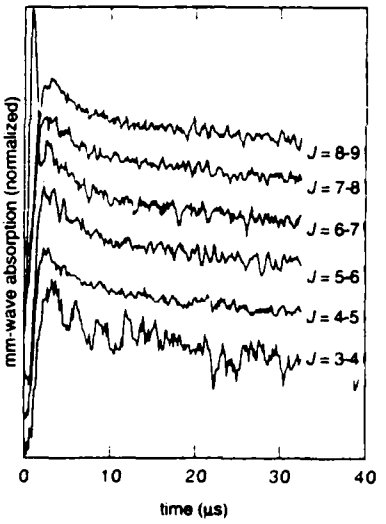

FIG. 7. IRMMDR time responses of CH_3Cl A-symmetry states in the $v_6=1$ vibrational manifold for $J=3-4$ to $8-9$. The time responses are offset vertically for legibility. All data are from $K=1$, $l=1$ using the $9P(26)$ pump line and a gas pressure of 50 mTorr. The spike at early time in $J=6-7$ is due to the a.c. Stark effect.

Even though the time responses of $9P(26)$ display a distinctive ETF, those within a nonpumped K/l stack have the same shape. Figure 7 further demonstrates this point. Given the mm/submm probe's sensitivity to nonthermal population distributions between adjacent J states, these data show that K-changing RET for a given K/l stack is very close to thermal. (4) *For 9P(26), the ETF is larger in low energy states.* At early time, more pump population that has undergone K-changing collisions is found in the $K'=0$ states ($K=-1$, $l=-1$ and $K=1$, $l=1$) than is found in $K'=6$ states ($K=5$, $l=-1$ and $K=7$, $l=1$). Since the changes in quantum number from the pumped to probed state are similar in both cases and the energies of the $K'=6$, K/l stacks are significantly higher than those of $K'=0$ and $K'=3$ (see Fig. 4), the ETF apparently has a stronger dependence on the state's rotational energy than on the state's angular momentum. (5) *For 9R(12), a wide range of states are populated thermally.* Figure 6 shows that K-changing RET in $9R(12)$ yields the same IRMMDR time responses for many different states. Picking the extremes of our measurements, the $J=4$, $K=1$, $l=1$ state (rotational energy 11 cm^{-1}) is populated at about the same rate as $J=9$, $K=5$, $l=-1$ (rotational energy 172 cm^{-1}). This is a clear demonstration that K-changing RET is not state specific. It transfers population over a change of $\Delta J=8$, $\Delta K=6$, $\Delta E=274$ cm^{-1} at a rate comparable to that of $\Delta J=3$, $\Delta K=2$, $\Delta E=113$ cm^{-1}.

VI. ANALYSIS

A. Generalized model for RET

The initial CH_3Cl analysis was performed using an adapted version of the computer program developed for the CH_3F analysis. The CH_3F model is represented schematically in Fig. 1. This successfully modeled collisional energy transfer in CH_3Cl, except that the state-dependent ETF of the

$9P(26)$ IRMMDR time responses could not be reproduced since the CH_3F model requires that all time responses be the same shape for all A states. However, a straightforward generalization of the K-changing RET process as modeled in CH_3F fully describes all of the features observed in the CH_3Cl data, including the ETF. In the CH_3F model, K-changing collisions distribute the population among the various J states according to a Boltzmann distribution at a *fixed* temperature, specifically, the temperature of the cell. For CH_3Cl, while K-changing RET still populates final states according to thermal Boltzmann statistics, the temperature of the population transferred by these collisions is initially some nonambient temperature that subsequently relaxes to the equilibrium temperature. The time dependence of this temperature is assumed to be

$$T(t)=T_e+(T_o-T_e)e^{-k_{T.R.}}, \tag{5}$$

where T_e is the equilibrium ambient temperature of the gas, T_o is the initial temperature of the pool, and $k_{T.R.}$ is the rate constant of the temperature relaxation.

A simple argument based on energy conservation motivates this modification of the model. Figure 4 shows the energies of the pumped states relative to room temperature thermal energy E_{kT}. At equilibrium, both partners in a collision come from a thermal distribution of rotational and translational energies. When the pump pulse populates a specific rotational state in the $v_6=1$ vibrational state, most of these pumped molecules still collide with molecules that are thermal since fewer than 1% of all molecules are excited by the pump. However, the pumped molecules are *not* thermal in their rotational energy. (They may also have a nonthermal translation energy which will be discussed later.) When the first K-changing collision occurs for a molecule pumped by the $9P(26)$ pump line, most of the nonthermal population is in only a few J states of $K=4$, $l=1$ since the dipole–dipole process is limited in range of J and is only marginally faster than the cumulative rate of K-changing collisions. The rotational energies of $J=5$–7 are between 79 and 91 cm^{-1}. While its collision partner is almost always a thermal ground state molecule, the initial state of the probed molecule is prepared by the pump to have one of these low rotational energies. Thus the average rotational energy available in the molecule's first K-changing collision is less than E_{kT}, so it is not surprising that the rotational distribution of final states from these collisions is at predominately lower energies.

For the $9P(26)$ pump line, the result of subsequent K-changing collisions is to raise the temperature of the A symmetry pool, so that the final temperature of the pool is the same as the cell temperature. As we argued above, the first K-changing collision of each pumped molecule leaves it in a lower energy state on average. However, the data indicate that the K-changing RET process in CH_3Cl is not state selective beyond the requirement that the initial temperature of the distribution be lower than the cell temperature; the final state of an individual rotational collision can be several J and K away from the initial state and can have a very different energy. Since almost all K-changing collisions involve thermal ground state molecules, K-changing collisions are efficient at uniformly raising the temperature of the cold

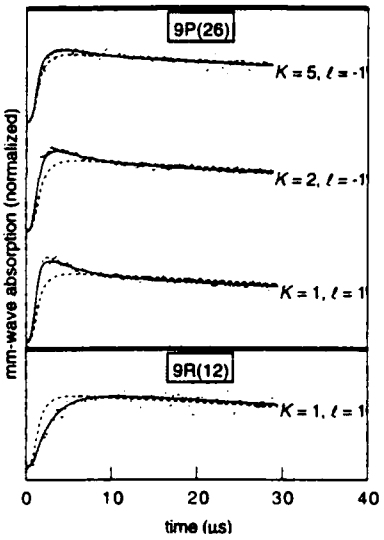

FIG. 8. Several $J=8$–9 IRMMDR time responses of K-changing collisions for $9P(26)$ and $9R(12)$ at 50 mTorr. One set of fitted time responses (dashed lines) shows the effect of fixing the temperature of the K-changing RET process to the cell temperature, while the other set (solid lines) comes from the generalized model where the temperature of transferred population decays to the cell temperature after starting at a nonambient initial temperature. The discrepancy in the first microsecond of the $9P(26)$ $K=2$, $l=-1$ time response is due to the Lorentzian tail of the much stronger signal at $K=4$, $l=1$.

A state distribution. In other words, the temperature of the A pool relaxes towards the cell temperature at a rate slightly slower than the cumulative rate of K-changing collisions because it takes a few of these collisions to cause the relaxation.

While the above argument was made for the $9P(26)$ pump line, the fact that the ETF is not discernible in the $9R(12)$ data is also consistent with this temperature–relaxing picture. Whereas K-changing RET for the $9P(26)$ pump initially concentrates the A pool population in the lowest rotational levels, K-changing collisions for the $9R(12)$ pump initially spread the pumped population over a larger number of A states due to the higher rotational energy of the state pumped by the $9R(12)$ coincidence. Just as for the case for the $9P(26)$ data, the A pool IRMMDR time responses initially rise as K-changing collisions populate A symmetry states with pumped molecules. However, in contrast to the $9P(26)$ data, the A pool time responses for $9R(12)$ continue to rise as the pool temperature relaxes *downward* towards cell temperature and the population increases in the measured rotational states. Because of the monotonic rise of these A symmetry time responses, the temperature relaxation does not cause a distinctive ETF such as that of the $9P(26)$ data.

This thermal K-changing RET process with a relaxing temperature is modeled in the following manner: the program initially calculates the total population that K-changing collisions put in all A states using the parameter $k_{\Delta K}$, which is the same for both pump states. The IRMMDR time response of a specific A symmetry transition is then calculated using this time–varying A pool population and the rotational

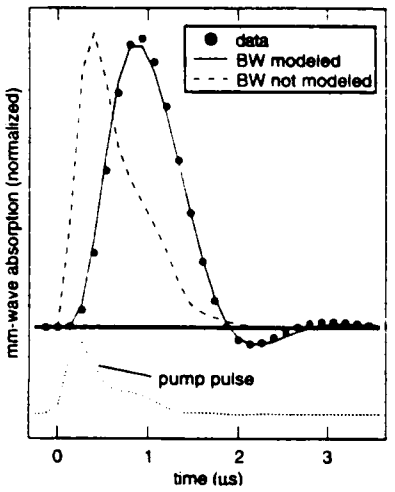

FIG. 9. Measured IRMMDR time response (dots) of the $J=6-7$, $K=4$, $l=1$ transition at 100 mTorr. The solid line is from a fit which includes detector bandwidth modeling, while the dashed line is based on a model that neglects the bandwidth effects. The digitized pump pulse of the $9P(26)$ line is shown at the bottom.

transition's time–varying absorption coefficient. The temperature dependence of a mm/submm absorption coefficient for CH_3Cl is given by

$$\alpha(t) \propto T^{-5/2} \exp\left(-\frac{E}{kT}\right), \tag{6}$$

where E is the rotational energy of the lower state and the limit $h\nu \ll E_{kT}$ has been used to simplify the expression.[45] The IRMMDR time response of a specific A symmetry transition is obtained by multiplying the population in the A pool transported by the K-changing rotational process by the ratio

$$\frac{\alpha(t)}{\alpha_e} = \left[\frac{T_e}{T(t)}\right]^{5/2} \exp\left\{\frac{E}{k}\left[\frac{1}{T_e} - \frac{1}{T(t)}\right]\right\}, \tag{7}$$

where T_e is the ambient temperature and $T(t)$ is the temperature of the population transported by K-changing collisions. The time dependence of $\alpha(t)$ is obtained by substituting Eq. (5) into Eq. (7). The modeled time responses shown in Fig. 6 were calculated using these equations. Figure 8 compares time responses of the unmodified CH_3F model (pool temperature fixed at ambient temperature) to those of the generalized model described above. Not only does this model correctly demonstrate the K-dependent ETF of the $9P(26)$ data, it also models the $9R(12)$ data, which does not demonstrate a distinctive ETF, using the same rate constant for K-changing collisions $k_{\Delta K}$ and the same relaxation rate constant for the temperature $k_{\text{T.R.}}$.

B. Other model modifications

Several sources contribute to the probe time responses that we measure: (1) population changes in either the upper or lower rotational level; (2) dephasing due to Doppler broadening and pressure broadening from both elastic and inelastic collisions; and (3) instrumental bandwidth. Thus far, we have been concerned with the source that most directly yields insight into RET—the population flow mechanisms. Fortunately, most of the time responses we acquired are dominated by collisional population flow; however, by correctly modeling the other two sources, the quality of the fits is significantly improved, especially when modeling J-changing collisions within a few J of the pumped state. One of the tests of the quality of the model is whether the rate constants are independent of pressure as they should be for two-body collisions. Correctly modeling the effects of Doppler and collisional dephasing as well as instrumental bandwidth reduced pressure dependencies in the fits and thus allowed us to apply the model over a larger pressure range when measuring the collision rates.

Figure 9 shows data significantly affected by the detector's bandwidth. At these higher pressures, where the rates are fastest, the IRMMDR time responses exhibit peak delay and overshoot characteristic of a two-pole lowpass filter. The detector's response is approximately

$$x(t) = C\int_{t-t'}^{t} f(t_o)\exp\left[-\frac{\gamma}{2}(t-t_o)\right] \times \sin\left[\frac{\sqrt{4\omega_o^2-\gamma^2}}{2}(t-t_o)\right]dt_o, \tag{8}$$

where $f(t)$ is the input signal measured by the detector and $t' = \max(20/\gamma, 0)$. We ignore the constant amplitude factor C since amplitude is a free parameter in our fits. The fit adjusted the oscillation parameter ω_o and decay parameter γ, resulting in values of 0.64 and 0.59 MHz, respectively. Although only the fastest IRMMDR time responses were significantly affected by the bandwidth (starting at about 20 mTorr for the states populated by J-changing collisions and at about 100 mTorr for those populated by K-changing collisions), by correctly modeling the detector bandwidth, we were able to fit data from a larger range of pressures.

At lower pressures, where the collisional rates are slowest, we observed another bandwidth limiting effect that is due to the molecules' polarization response times. This may be thought of as the time it takes the induced dipoles, the pumped nonthermal molecules, to align with the probe field. The response may be derived using the density operator formalism.[46] For our typical probe intensity, the Rabi frequency is $8000/2\pi$ Hz, which is slow compared to the time scales of our measurements and is much slower than the dephasing rates; therefore, the calculation is performed in the limit that the Rabi frequency is much longer than the relaxation rates. We want to find the time-dependent absorption $\alpha(t)$ of the probe field

$$\frac{dP}{dz} = -\alpha(t)P, \tag{9}$$

where z is the direction of propagation of the radiation along the axis of the absorption cell and P is the mm/submm probe power. The electric field in the molecular frame is

$$\mathbf{E}(v,t) = \tfrac{1}{2}E_0(t)\hat{\mathbf{e}}e^{-i(\omega-kv)t} + \text{c.c.} = \tfrac{1}{2}\mathscr{E}(t)e^{-i(\omega-kv)t} + \text{c.c.} \tag{10}$$

and the polarization is

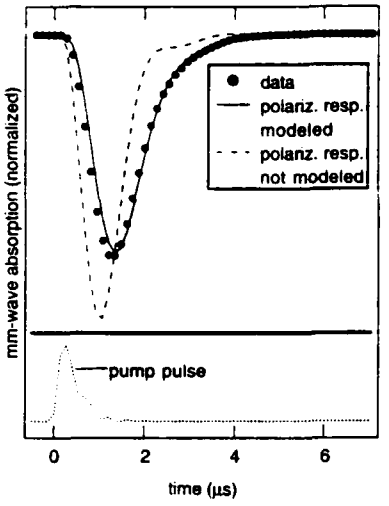

FIG. 10. Measured IRMMDR time response (dots) of the $J=5-6$, $K=4$, $l=1$ transition at 20 mTorr. The solid line is based on the complete model which includes the modeling of polarization response time, while the dashed line is based on a model which neglects polarization delay. The digitized pump pulse of the $9P(26)$ line is shown at the bottom.

$$\mathbf{P}(v,t)=\tfrac{1}{2}\mathscr{P}(v,t)e^{-i(\omega-kv)t}+\text{c.c.}, \tag{11}$$

where $\mathscr{E}(t)$ and $\mathscr{P}(v,t)$ are the slowly varying amplitudes in the molecule frame. The power per unit volume absorbed from the probe field as measured by the detector is

$$\frac{dP}{dV}=\frac{dI}{dz}=-\int dv\langle\dot{\mathbf{P}}(v,t)\cdot\mathbf{E}(v,t)\rangle_t$$

$$=-\frac{1}{2}\int dv\ \mathrm{Re}[-i\omega\mathscr{E}^*(t)\cdot\mathscr{P}(v,t)], \tag{12}$$

where V is the cell volume and I is the probe intensity. The velocity integration is performed over the probed velocity subclass. The polarization may be derived using the equation of motion for the density matrix ρ,

$$\dot{\rho}(v,t)=-\frac{i}{\hbar}\ [H,\rho(v,t)], \tag{13}$$

where $H=H^{(0)}-\boldsymbol{\mu}\cdot\mathbf{E}(t)$ and the density operator is a function of molecular velocity v and time. Labeling the lower and upper probe states 1 and 2, respectively, we expand Eq. (13) and modify the result to include decay from dephasing collisions

$$\dot{\rho}_{21}(v,t)=-(\gamma_{\text{P.B.}}+i\omega_{21})\rho_{21}+\frac{i}{\hbar}\ \boldsymbol{\mu}_{21}\cdot\mathbf{E}(v,t)[\rho_{11}(v,t)$$

$$-\rho_{22}(v,t)], \tag{14}$$

$$\dot{\rho}_{12}(v,t)=\dot{\rho}^*_{21}(v,t)$$

where ω_{21} is the mm/submm transition frequency between the rotational levels and $\gamma_{\text{P.B.}}$ is the half-width at half-maximum (HWHM) pressure broadening rate in radians per seconds. The solution to Eq. (14) in the rotating wave approximation is

$$\rho_{21}(v,t)=i\ \frac{\boldsymbol{\mu}_{21}\cdot\hat{\mathbf{e}}E_0}{2\hbar}\int_{-\infty}^{t}dt'\ \exp[-(\gamma_{\text{P.B.}}+i\omega_{21})(t-t')]$$

$$\times\exp[-i(\omega-kv)t'][\rho_{11}(v,t')-\rho_{22}(v,t')],$$

$$\rho_{12}(v,t)=\rho^*_{21}(v,t). \tag{15}$$

The polarization is given by

$$\mathbf{P}(v,t)=\mathrm{Tr}[\boldsymbol{\mu}\rho(v,t)]=2\ \mathrm{Re}[\boldsymbol{\mu}_{12}\rho_{21}(v,t)]. \tag{16}$$

Compared to Eq. (11), the slowly varying amplitude of the polarization can be written as

$$\mathscr{P}(v,t)=2\boldsymbol{\mu}_{12}\rho_{21}(v,t)e^{i(\omega-kv)t}. \tag{17}$$

Rearranging Eq. (9) and substituting Eqs. (12), (15), and (17) yields the general expression for the time dependence of the absorption coefficient

$$\alpha(t)=\frac{4\pi k|\boldsymbol{\mu}_{21}\cdot\hat{\mathbf{e}}|^2}{\hbar}\ \mathrm{Re}\left(\int dv\int_{-\infty}^{t}dt'\right.$$

$$\times\exp\{-[\gamma_{\text{P.B.}}+i(\Delta-kv)](t-t')\}[\rho_{11}(v,t')$$

$$\left.-\rho_{22}(v,t')]\right), \tag{18}$$

where $\Delta\equiv\omega_{12}-\omega$ and $k=\omega c^{-1}$. For $\Delta=0$ and assuming a thermal distribution of molecular velocities, i.e., $\rho_{11}(v,t)=\rho_{11}(t)(u\sqrt{\pi})^{-1}\exp(-v^2/u^2)$, this reduces to

$$\alpha(t)=\frac{4\pi k|\boldsymbol{\mu}_{21}\cdot\hat{\mathbf{e}}|^2}{\hbar}\ \mathrm{Re}\left\{\int_{-\infty}^{t}dt'e^{-\gamma_{\text{P.B.}}(t-t')}\right.$$

$$\left.\times\exp\left[-\left(\frac{1}{2}\ ku\right)^2(t-t')^2\right][\rho_{11}(t')-\rho_{22}(t')]\right\}, \tag{19}$$

where $u=\sqrt{2kT/M}$ is the thermal speed of the molecules along the axis of the absorption cell. The effect that the polarization response has on a pumped K/l stack IRMMDR time response is shown in Fig. 10. This model is not complete since it assumes a thermal velocity distribution for molecules; nonetheless, including this polarization effect in the model significantly improved the quality of the fits without adding any adjustable parameters. Data significantly affected by nonthermal velocity distributions were excluded from the fits, specifically, low pressure J-changing RET data near the pumped state. Allowing the model to adjust the pressure broadening parameter in Eq. (19) resulted in the value $\gamma_{\text{P.B.}}=15$ MHz/Torr, which agrees well with pressure broadening coefficients based on linewidth measurements; therefore, $\gamma_{\text{P.B.}}$ was fixed to this value.

In order to ensure that no pertinent early time information was inadvertently lost as a result of undersampling, we typically used digitization rates of 0.133 and 0.333 μs when acquiring IRMMDR time responses. When analyzing the data, we employed a scheme to eliminate oversampled data points from the fit to reduce computer run times. This was accomplished by programming the computer model to apply a boxcar averager with a window size depending on the frequency content of the data trace at a given time. Problems

with changing the phase of the signals were avoided by applying the boxcar averager to the measured time responses after simulated time responses had already been subtracted from them in preparation for the least squares fit routine. The windows were required to be narrow enough that the filter affected fitted parameters by no more than one part in 10^5. Even with this stringent constraint, many fit times were reduced by more than 90%.

C. Application of the model

Excluding data acquired with various pump frequency and probe frequency offsets (used for observing velocity subclass effects), there were 1027 IRMMDR time responses available for the $CH_3\,^{35}Cl$ analysis. Where redundant time responses existed (same pump line, probe line, and pressure), the one with the best signal to noise ratio was chosen, leaving 579 time responses for 64 probe transitions and two pump coincidences. Most probe transitions were measured for both pump states, and most time responses were taken at six to eight different pressures. After eliminating the IRMMDR time responses with inadequate signal to noise ratios and many of the time responses for vibrational processes, there were 366 time responses that were weighted in the fits according to their signal to noise levels.

To determine the collision rates for CH_3Cl, IRMMDR time responses were grouped by pool or included as individual J states for the pumped K/l stack, then the following sequence applied: (1) a large set of time responses over the full range of pressures (up to 297 time responses simultaneously) was fit by adjusting the appropriate parameters. Eventually, all data were grouped into two sets (one for all time responses of states in the same K/l stacks as the pumped states and one for all other data). Since the program runs much faster when the individual J states are not included, the model used individual J states only for J-changing data and the faster model using only pools of states was used for all other time responses. (2) A data set was subdivided into groups with the same pressure and then were fit separately to check for any pressure dependence in the parameters. (3) Since pressure variations in the fitted rate constants indicate a systematic experimental or modeling problem, data for any fits demonstrating deviations with pressure at either low or high pressures are eliminated. However, the model was found to be valid over a large pressure range and only 16 time responses for some transitions in the pumped K/l stack at low pressures were eliminated due to significant collisionless effects. (4) Finally, the fit was run again using the entire data set to arrive at the final parameters.

These steps were performed for each group of data and then the whole process was repeated until the fit error was minimized. The final fit parameters represent 350 IRMMDR time responses grouped in two sets, each of which were fit simultaneously—53 time responses representing J-changing RET and 297 time responses representing K-changing RET and the vibrational processes. For K-changing RET and vibrational processes, the model was found to be valid over the full pressure range used to acquire data, 1–100 mTorr for K-changing RET and 20–1000 mTorr vibrational processes.

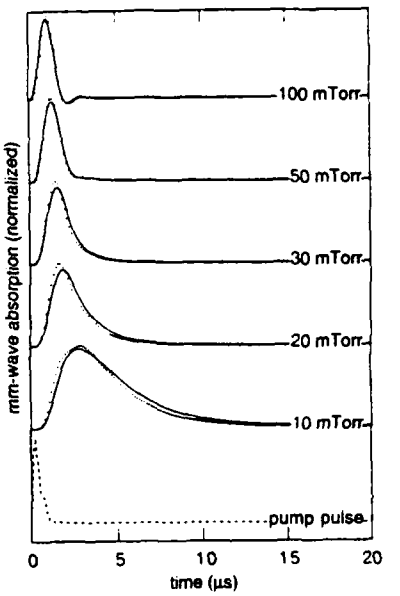

FIG. 11. Measured IRMMDR time response (dots) of the $v_6=1$, $J=7$–8, $K=4$, $l=1$ transition at several pressures. The solid lines are based on the complete model using the IOS-P law for J-changing collisions. The digitized pump pulse of the $9P(26)$ line is shown at the bottom.

For J-changing RET, the dipole–dipole process and the scaling laws were applied to the IRMMDR time responses of the pumped K/l stacks to determine the best method of modeling J-changing collisions. Four permutations of the model were run using three groupings of the data [only $9P(26)$ data, only $9R(12)$ data, and both simultaneously] to determine the best model—the SPG law with and without a separate dipole–dipole process and similarly the IOS-P law with and without a separate dipole–dipole process. When the dipole–dipole process was included in the model, the scaling law was used for only higher-order collisions $\Delta J \geq 2$; otherwise, the scaling law included $\Delta J \geq 1$. The parameters for the bandwidth modeling and the polarization response were also adjusted in these ΔJ fits and the resulting parameters were then used for all subsequent fits. We came to several conclusions. First, both the SPG and IOS-P scaling laws accurately model the data with the latter resulting in a slightly better figure of merit. Also, we found that fitting separately for the dipole–dipole process did not significantly improve the qual-

TABLE II. RET fit parameters.

Parameter	Fit result[a]	Cross section (Å^2)
$k_{\Delta K}$	11.1±0.8 $\mu s^{-1}Torr^{-1}$	69±5
$T_{o,9P(26)}$	138±6 K	
$T_{o,9R(12)}$	374±17 K	
k_{TR}	7.5±0.2 $\mu s^{-1}Torr^{-1}$	47±1
k_{dd}	48±2 $\mu s^{-1}Torr^{-1}$	299±9
IOS-P c	21.7±1.1 $\mu s^{-1}Torr^{-1}$	134±7
γ	1.23±0.02	
SPG c	0.0120±0.0006 $\mu s^{-1}Torr^{-1}$	0.074±0.005
γ	1.12±0.01	

[a]Errors are 2.5 times σ from the nonlinear least squares fit routine.

ity of the fits and is therefore unnecessary to include in the model. That is, either the SPG or IOS-P scaling law accurately accounts for the $\Delta J=\pm 1$ collisions in addition to the higher-order $|\Delta J|\geq 2$ collisions. Examples of the fits using the IOS-P model are shown in Figs. 5 and 6 for different J states and in Fig. 11 at different pressures. The total rate constants for dipole–dipole collisions using the branching ratios of Eq. (1) is $k_{dd}=48\ \mu s^{-1}\ Torr^{-1}$, about six times the gas kinetic collision rate constant.

In the previously reported analysis of the CH_3F data,[6] the dipole–dipole process was included separately. However, with the improved bandwidth modeling and the new polarization response modeling in the revised model discussed here, a reanalysis of the data used in the previous paper indicates that a separate dipole–dipole process is unnecessary for CH_3F as well. These findings will be reported in detail in a future paper.

The resulting RET parameters for both J- and K-changing collisions are listed in Table II. Rates are converted to cross sections using the relation

$$k=n\langle v_{rel}\rangle\sigma,$$

where n is the number of molecules per volume and $\langle v_{rel}\rangle$ is the average relative velocity of the collision partners. The average relative velocity for the Maxwell–Boltzmann distribution is

$$\langle v_{rel}\rangle=\sqrt{16kT/\pi m}.$$

All parameters come from fits simultaneously including data from both pump coincidences. The scaling law parameters for both the SPG and IOS-P models come from fits where the selected scaling law modeled all J-changing processes including those with dipole–dipole selection rules. The k_{dd} parameter comes from a fit where the IOS-P law modeled all other J-changing collisions, specifically $|\Delta J|\geq 2$, while Eq. (1) was used for $\Delta J=\pm 1$.

D. Other possible sources of ΔK signal considered

Since a central result of this study is the generalization of the thermal K-changing rotational process to accurately model the data for both pump coincidences, it is important to consider other possible sources of the ETF. One such source is velocity subclass effects. The center frequencies of the pump transitions do not exactly match the center frequencies of the pumped CH_3Cl rovibrational transitions—the laser frequency mismatches are 20 MHz for the $9P(26)$ coincidence with $CH_3{}^{35}Cl$ and -30 MHz for $9R(12)$.[47] Since the CH_3Cl infrared transitions are inhomogeneously broadened in our pressure range, the molecules that are pumped are those with the velocity that provides the needed Doppler shift to correct for this frequency mismatch. The pumped molecules retain this nonthermal velocity distribution until thermalized by gas kinetic collisions. Since the dipole–dipole and cumulative rate for K-changing collisions are comparable to or faster than the gas kinetic collision rate, many molecules undergo a change in rotational state before their velocity distribution is thermalized. So the frequency spike that is observable in the probe frequency profiles of the three level double resonance measurements may also be observed for other probe transitions, specifically, transitions in the pumped K/l stack and to a lesser degree all transitions of the same symmetry as the pumped state. In their infrared/infrared double resonance study of CH_3F, Song and Schwendeman observed these spikes in the frequency profiles of IRIRDR measurements of the pumped K stack.[15] Everitt also observed this effect for both J- and K-changing collisions in time-resolved IRMMDR measurements.[37] To investigate the possibility that the ETF of the CH_3Cl data is due to this velocity subclass effect IRMMDR time responses were taken over a grid of pump and probe frequencies. For our mm/submm probe frequencies, it is only at pressures less than about 10 mTorr that pressure broadening becomes smaller than Doppler broadening. Although there is marginal evidence for an early-time probe frequency asymmetry in the A transitions at lower pressures, the size of the effect is clearly smaller than the ETF of Fig. 6. Furthermore, the fact that the magnitude of the ETF increases at higher pressures is not consistent with attributing the ETF to velocity effects. Moreover, the absence of the ETF in the $9R(12)$ data is not consistent with attributing the ETF to velocity subclass effects.

We also attempted to account for the ETF of the $9P(26)$ IRMMDR time responses by breaking K-changing RET into separate processes $K'=3\rightarrow 0$, $K'=3\rightarrow 6$, and $K'=0\rightarrow 6$. As with the CH_3F model, the individual $\Delta K'$ processes were defined to be thermal in J with the temperature fixed at the cell temperature. The reasoning behind the model was that the ETF for the $K'=0$ and $K'=3$ data might be caused by population initially entering these states quickly then moving into $K'\geq 6$ states more slowly. Although such a model can qualitatively account for some of the features observed in the data, it could not reproduce the IRMMDR time responses due to the following competing effects: the individual $\Delta K'$ rates would have to be close enough to each other to account for the similar rise times of $K'=0$, 3, and 6 transitions, but at the same time different enough to allow for the fall of the ETF in the $K'=0$ and 3 data that is absent in the $K'=6$ data. Given the equilibrium percentage of population in $K'\geq 6$ relative to all $v_6=1$, A symmetry states (31%), no combination of rates could account for the ETF in the $K'=0$ and 3 states. Further subdividing the $\Delta K'$ process into more state-specific processes also failed to overcome this difficulty.

VII. DISCUSSION

A. Comparison of CH_3Cl and CH_3F

Within the expected rate constant variations, the rotational processes in CH_3Cl are for the large part the same as those of CH_3F. The dipole–dipole process has the fastest state-to-state rates in both molecules; however, other RET processes in both molecules play more important roles in the thermalization of the rotational states in the pumped vibrational manifold since they have larger ranges in ΔJ and permit K-changing collisions. Higher-order J-changing collisions in both molecules populate states in the pumped K stack (or K/l stack for $v_6=1$ in CH_3Cl) that are more than several J away from the pumped state more quickly than multiple dipole–dipole collisions because they have a larger range in J. In addition, the thermal K-changing RET process

in both molecules exhibits state-to-state rates very different in character than those of J-changing collisions. Although some of the double resonance signals for CH_3Cl and CH_3F appear to be quite different, this disparity can be explained by a difference in the temperatures at which K-changing collisions populate states of the pumped symmetry in the two molecules.

Due to the similarity of the molecules, the generalized model developed for CH_3Cl should also apply to CH_3F. In fact, a preliminary reanalysis of the CH_3F data indicates that the generalized model is consistent with CH_3F. However, the previous work[5] found that a model using a fixed 300 K temperature for the thermal Boltzmann distribution of final states was sufficient for modeling K-changing collisions in CH_3F, whereas fixed temperature models fail for CH_3Cl. Several reasons for this follow: First, since the B rotational constant for CH_3Cl is nearly half the value of B for CH_3F, while their A rotational constants are nearly equal, there are many more thermally populated J states for a given K in CH_3Cl than in CH_3F. Consequently, CH_3Cl provides a more severe test of the thermal nature of K-changing RET since large changes in the angular momentum of the pumped population are required to warm or cool the population distribution of A pool states to room temperature. Second, the available CO_2–CH_3Cl pump coincidences populate rovibrational states that are more widely spaced in rotational energy than those of CH_3F. For CH_3Cl, the pumped rovibrational states have rotational energies of 85 cm^{-1} for $9P(26)$ and 285 cm^{-1} for $9R(12)$, while for CH_3F, the pumped rovibrational states have rotational energies of 64 cm^{-1} for $9P(32)$ and 148 cm^{-1} for $9P(20)$. This difference of pumped state rotational energies in CH_3Cl and the fact that one is larger than room temperature thermal energy while the other is smaller enhances the differences the molecules exhibit in K-changing collisions. Last, a secondary pump coincidence for the $9P(20)$ pump line noticeably affects early times in IRMMDR time responses needed for measuring K-changing collisions in $K=1$ of $^{12}CH_3F$.

B. Comparison with NH_3

In addition to the CH_3F work[5] and the present study, the work of Abel *et al.* for NH_3 provides detailed measurements of state-to-state rates for K-changing collisions for a symmetric top molecule.[29] Using a time-resolved IRIRDR technique, they probed the time responses of several rotationally resolved $2\nu_2 \leftarrow \nu_2$ transitions in NH_3 as the states responded to excitation by the $10P(32)$ line of a CO_2 laser. This pump coincidence populates the a inversion level of $\upsilon_2=1$, $J=5$, $K=3$. They probed several rotational states of opposite parity—six J levels in $K=3$ and eight J levels in $K=0$. This allowed them to calculate the state-to-state RET rate constants for several $\Delta K=0$ and -3 collisional processes using a master-equation model for RET. In their model, the $\Delta K=0$ processes were calculated using the EGL fitting law, but the $\Delta K=-3$ processes were fitted individually since neither the EGL nor SPG law could reproduce satisfactorily the IRIRDR time responses. They grouped many rotational states with larger J or K into four pools of states to reduce the total number of states in their model since, in the absence of a scaling relation for K-changing collision rates, each additional state adds a free parameter to the master equation.

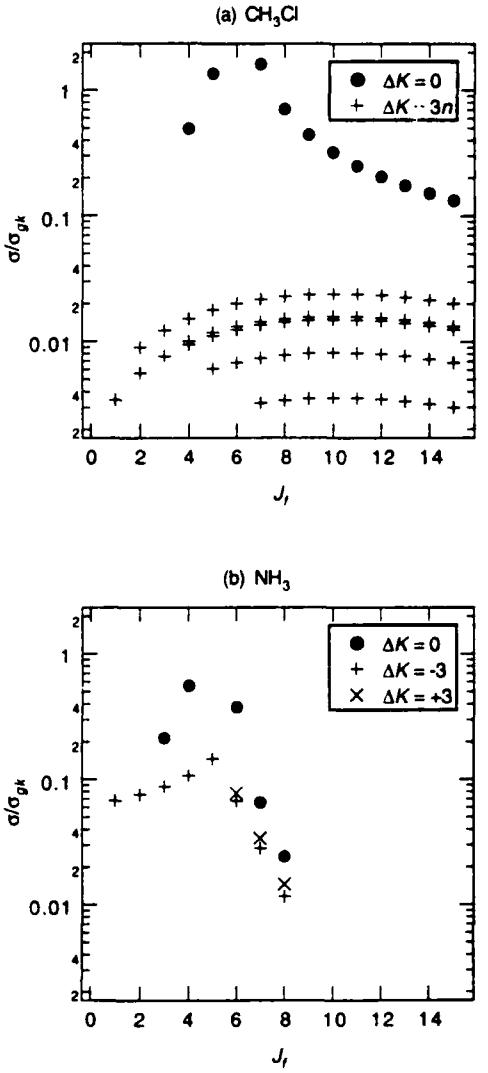

FIG. 12. State-to-state collision cross sections for rotational collisions in (a) CH_3Cl using the $9P(26)$ pump line and (b) parity-changing rotational collisions measured by Abel *et al.* (Ref. 29) for NH_3. The cross sections are normalized to each molecule's gas kinetic cross section. The initial state for CH_3Cl is $\upsilon_6=1$, $J=6$, $K=4$, $l=1$ and the initial state for NH_3 is the a inversion level of $\upsilon_2=1$, $J=5$, $K=3$.

It is interesting to compare the magnitudes of the state-to-state collision rate constants for CH_3Cl and NH_3, bearing in mind that while both molecules are symmetric tops, NH_3 has the additional degree of freedom from inversion. Abel *et al.* found that both parity-changing (inversion state-changing) and parity-conserving (inversion state-conserving) collisions occurred and modeled them by assuming their rates are different by a ratio $\beta=k(a\leftrightarrow a)/k(a\leftrightarrow s)=k(s\leftrightarrow s)/k(a\leftrightarrow s)$, which was found to be greater than 0.7. Figure 12 compares the state-to-state rate constants for parity-changing collisions in NH_3 measured by Abel *et al.* with the state-to-state rate constants for collisions in CH_3Cl calculated using our five parameter model for RET. The rates

have been normalized to the gas kinetic collision cross sections for each molecule.

Remembering that $J_i=J_{pump}=6$ for CH_3Cl and $J_i=J_{pump}=5$ for NH_3, Fig. 12 shows that for both molecules, the largest state-to-state rates are those with dipole–dipole selection rules. In addition, for NH_3, the fastest $\Delta K=-3$ state-to-state rate is $\Delta J=0$ and the rates decrease with larger $|\Delta J|$, indicating a propensity for RET processes to conserve angular momentum in the pumped molecule during K-changing collisions. In contrast, the state-to-state rates for CH_3Cl K-changing collisions are maximum at $J=10$ rather than $J=6$ because for this molecule K-changing RET is thermal; $J=10$ corresponds to the maximum in the Boltzmann distribution for the 138 K initial temperature of the $9P(26)$ pump coincidence shown in Table II. Final states at smaller J_f receive less population because their $(2J+1)$ M-degeneracies are small, while states at larger J_f receive less population due to the exponential rolloff of the Boltzmann distribution with energy.

Figure 12 shows that the J-changing collisions in CH_3Cl are faster than the fastest K-changing collisions by a factor of about 10 (for large ΔJ) to 100 (for small ΔJ), whereas in NH_3, $\Delta K=0$ collisions are only two to three times faster than $\Delta K=-3$ collisions. These ratios can be understood from the physical structures of the two molecules using the following classical picture: collisions that change K for both CH_3Cl and NH_3 require a collision of hydrogen atoms since they provide the off-axis structure for these symmetric tops. The center of mass for NH_3 is near the nitrogen nucleus, and the rotational constants for NH_3 are large and similar in value ($B\approx300$ GHz and $C\approx190$ GHz); thus, the moment of inertia for rotation about the symmetry axis is not significantly different than the moment of inertia about a perpendicular axis for tumbling motion. While J-changing collisions can occur for long-range, dipole–dipole interactions of NH_3 molecules, K-changing collisions require short-range, higher-order interactions closer to the repulsive portion of the intermolecular potential. During such a hard collision between the partner and a hydrogen atom of NH_3, it is about equally likely that the molecule's angular momentum about the symmetry axis will change as for an axis of tumbling motion because the line defined by the point of contact and the molecule's center of mass approximately bisects the angle between these two rotation axes. Therefore, while $\Delta K=0$ state-to-state rates can be expected to be larger since the dipole–dipole interaction between the colliding molecules do not require small impact parameters, during short-range collision of NH_3 molecules where higher-order multipoles can be significant, J- and K-changing collisions are roughly equally likely for NH_3 as observed in Fig. 12.

The structure of CH_3Cl is different than that of NH_3. The center of mass for CH_3Cl is near the heavy chlorine nucleus and the moments of inertia are different by more than a factor of 10 ($B\approx13$ GHz and $A\approx150$ GHz). So a hard collision between a partner and a hydrogen atom in a CH_3Cl molecule, the type of collision required to change K, is more likely to change the angular momentum about an axis for tumbling motion than about the symmetry axis since the molecule's center of mass is at the opposite end of the molecule. In other words, a CH_3Cl collision that changes K is likely to have caused an even larger change in J. In fact, such large changes in J occur that the K-changing process in CH_3Cl can be treated as a thermal process.

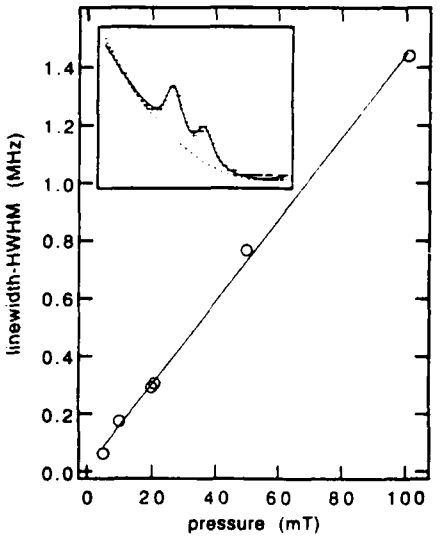

FIG. 13. Measured pressure broadening linewidths vs pressure for the $v_6=1$, $J=6$–7, $K=4$, $l=1$ transition. The inset shows one of the frequency profiles taken at 20 mTorr. The Voigt line shape was used with the Gaussian component fixed at 0.163 MHz. Both the intercept and slope were free variables in the linear fit, resulting in a pressure broadening coefficient of 14.3±1.0 MHz/Torr.

C. A comparison of collision rates with pressure broadening

An important cross check of the accuracy of the measured state-to-state collision rates is a comparison of the pressure broadening derived from the individual rate constants with the measured pressure broadening coefficients. For CH_3Cl, the cumulative depopulation rate of the $9P(26)$ pumped state through $\Delta K=0$ channels is 85 μs^{-1} $Torr^{-1}$ based on an IOS-P law summation. This includes the $\Delta J=0$, $\Delta K=0$ elastic collision rate that is calculated using the branching ratios for dipole–dipole collisions found in Eq. (1). It is interesting to note the total rate constant for dipole–dipole collisions is 48 μs^{-1} $Torr^{-1}$, only 57% of all $\Delta K=0$ collisions. As shown in Table II, the cumulative rate constant for K-changing collisions is 11.1 μs^{-1} $Torr^{-1}$. The equation used to calculate pressure broadening in MHz/Torr is

$$\gamma/p=(1/2\pi)(k_u+k_l)/2, \tag{20}$$

where p is the pressure in Torr and the cumulative depopulation rate constants for the upper and lower transition levels k_u and k_l are expressed in μs^{-1} $Torr^{-1}$. Including the small contributions from the vibrational processes, the fit parameters result in a pressure broadening coefficient of 12.9±0.5 MHz/Torr. We have performed a series of pressure broadening measurements on a transition involving the pumped state $v_6=1$, $J=6\rightarrow7$, $K=4$, $l=1$. The data are plotted in Fig. 13

and the resulting pressure broadening parameter of 14.3 ± 1.0 MHz/Torr agrees well with the parameter determined from the rate constants.

VIII. CONCLUSIONS

To summarize, we report that all state-to-state rotational energy transfer processes in $v_6 = 1$ of CH_3Cl can be described in terms of a small number of physically meaningful parameters. The CH_3Cl state-to-state rotational collision rates from either of the two pumped states to any other A symmetry rotational state in $v_6 = 1$ may be calculated using the RET model described in this paper and measured parameters of Table II. For each pump state, only five parameters are needed to model all of these state-to-state rates—two parameters for either the SPG or IOS-P scaling law for J-changing RET and three parameters for the temperature-relaxing, thermal K-changing process. Furthermore, four of these parameters are the same for all initial states; only the initial temperature of the thermal K-changing process varies with initial state.

It should be emphasized that these parameters account correctly for a large number of experimental double resonance time responses (which often have very different shapes) taken over a wide range of parameter space. Specifically, 350 IRMMDR time responses were used with pressures ranging from 1 to 100 mTorr (20 to 1000 mTorr for states populated by vibrational processes) for 43 probe transitions covering a wide range of J and K, pumped and unpumped symmetry species, and two different pump states. As for our earlier CH_3F (Refs. 5 and 6) study, the statistical power gap fitting law and the infinite order sudden approximation using a power law expression for the basis rates accurately model J-changing ($\Delta K = 0$) collisions. Furthermore, the intermolecular potentials for these two methyl halides result in K-changing collision rates that can be modeled very simply. The state-to-state rates to all eligible final states (i.e., states of the same symmetry and vibrational energy as the pumped state) are such that the pumped population transferred to these states is distributed according to a Boltzmann distribution even at the earliest times. The most significant difference between rotational energy transfer in these two molecules is that whereas a temperature fixed at the ambient temperature of the cell was found to be sufficient for modeling K-changing collisions in CH_3F, the CH_3Cl data required a time-varying temperature. However, both parameters for this temperature are closely related to other known physical characteristics of the molecule—the initial temperature is related to the rotational energy of the pumped state and the rate of the temperature's exponential relaxation back to the ambient temperature of the cell is slightly less than the cumulative rate of K-changing collisions.

ACKNOWLEDGMENTS

The authors thank the Army Research Office for supporting this work. We also express appreciation to Dr. Henry Everitt for many insightful conversations and to Dr. John Thomas for his help in modeling the polarization response.

[1] W. H. Matteson and F. C. De Lucia, IEEE J. Quantum Electron. **19**, 1284 (1983).
[2] W. H. Matteson and F. C. De Lucia, J. Opt. Soc. of Am. B **2**, 336 (1985).
[3] R. I. McCormick, F. C. De Lucia, H. O. Everitt, and D. D. Skatrud, IEEE J. Quantum Electron. **23**, 2069 (1987).
[4] R. I. McCormick, F. C. De Lucia, and D. D. Skatrud, IEEE J. Quantum Electron. **23**, 2060 (1987).
[5] H. O. Everitt and F. C. De Lucia, J. Chem. Phys. **90**, 3520 (1989).
[6] H. O. Everitt and F. C. De Lucia, J. Chem. Phys. **92**, 6480 (1990).
[7] H. O. Everitt and F. C. De Lucia, Mol. Phys. **79**, 1087 (1993).
[8] T. Oka, in *Advances in Atomic and Molecular Physics*, edited by D. R. Bates and I. Estermann (Academic, New York, 1973), Vol. 9, pp. 127–206.
[9] L. Frenkel, H. Marantz, and T. Sullivan, Phys. Rev. A **3**, 1640 (1971).
[10] C. Douketis, T. E. Gough, G. Scoles, and H. Wang, J. Phys. Chem. **88**, 4484 (1984).
[11] Y. Matsuo and R. H. Schwendeman, J. Chem. Phys. **91**, 3966 (1989).
[12] U. Shin and R. H. Schwendeman, J. Chem. Phys. **94**, 7560 (1991).
[13] U. Shin, Q. Song, and R. H. Schwendeman, J. Chem. Phys. **95**, 3964 (1991).
[14] Q. Song and R. H. Schwendeman, J. Mol. Spectrosc. **153**, 385 (1992).
[15] Q. Song and R. H. Schwendeman, J. Chem. Phys. **98**, 9472 (1993).
[16] R. Goldflam, S. Green, and D. J. Kouri, J. Chem. Phys. **67**, 4149 (1977).
[17] T. A. Brunner, R. D. Driver, N. Smith, and D. E. Pritchard, Phys. Rev. Lett. **41**, 856 (1978).
[18] T. A. Brunner, R. D. Driver, N. Smith, and D. E. Pritchard, J. Chem. Phys. **70**, 4155 (1979).
[19] S. Green, J. Chem. Phys. **70**, 816 (1979).
[20] M. Wainger, I. Al-Agil, T. A. Brunner, A. W. Karp, N. Smith, and D. E. Pritchard, J. Chem. Phys. **71**, 1977 (1979).
[21] T. A. Brunner, N. Smith, A. W. Karp, and D. E. Pritchard, J. Chem. Phys. **74**, 3324 (1981).
[22] N. Smith and D. E. Pritchard, J. Chem. Phys. **74**, 3939 (1981).
[23] H. Du, D. J. Krajnovich, and C. S. Parmenter, J. Phys. Chem. **95**, 2104 (1991).
[24] T. Oka, J. Chem. Phys. **48**, 4919 (1968).
[25] *D. Harradine, B. R. Foy, L. Laux, M. Dubs, and J. I. Steinfeld*, J. Chem. Phys. **81**, 4267 (1984).
[26] B. J. Orr, J. G. Haub, and R. Haines, Chem. Phys. Lett. **107**, 168 (1984).
[27] B. R. Foy, J. R. Hetzler, G. Millot, and J. I. Steinfeld, J. Chem. Phys. **88**, 6838 (1988).
[28] J. R. Hetzler and J. I. Steinfeld, J. Chem. Phys. **92**, 7135 (1990).
[29] B. Abel, S. L. Coy, J. J. Klaassen, and J. I. Steinfeld, J. Chem. Phys. **96**, 8236 (1992).
[30] S. Kano, T. Amano, and T. Shimizu, Chem. Phys. Lett. **25**, 119 (1974).
[31] C. P. Bewick, J. G. Haub, R. G. Hynes, J. F. Martins, and B. J. Orr, J. Chem. Phys. **88**, 6350 (1988).
[32] B. J. Orr, Int. Rev. Phys. Chem. **9**, 67 (1990).
[33] R. Dopheide, W. B. Gao, and H. Zacharias, Chem. Phys. Lett. **182**, 21 (1991).
[34] R. Parson, J. Chem. Phys. **93**, 8731 (1990).
[35] R. Parson, J. Chem. Phys. **95**, 8941 (1991).
[36] B. R. Foy, L. Laux, S. H. Kable, and J. I. Steinfeld, Chem. Phys. Lett. **118**, 464 (1985).
[37] H. O. Everitt, Ph.D. thesis, Duke University, 1990.
[38] C. H. Townes and A. L. Schawlow, *Microwave Spectroscopy* (Dover, New York, 1955), p. 74.
[39] W. C. King and W. Gordy, Phys. Rev. **90**, 319 (1953).
[40] P. A. Helminger, F. C. De Lucia, and W. Gordy, Phys. Rev. Lett. **25**, 1397 (1970).
[41] P. A. Helminger, J. K. Messer, and F. C. De Lucia, Appl. Phys. Lett. **42**, 309 (1983).
[42] S. L. Coy, S. D. Halle, J. L. Kinsey, and R. W. Field, J. Mol. Spectrosc. **153**, 340 (1992).
[43] S. Kondo, Y. Koga, and T. Nakanaga, Chem. Soc. Jpn. **58**, 65 (1985).
[44] S. Kondo, Y. Koga, and T. Nakanaga, J. Phys. Chem. **90**, 1519 (1986).
[45] W. Gordy and R. L. Cook, *Microwave Molecular Spectra*, 3rd ed. (Wiley, New York, 1984), Vol. 18, p. 209.
[46] J. E. Thomas (private communication).
[47] J.-C. Deroche and G. Graner, in *Optically Pumped Far-Infrared Lasers*, edited by K. J. Button, M. Inguscio, and F. Strumia (Plenum, New York, 1984), Vol. 2, pp. 35–42.